Online damage detection via a synergy of proper orthogonal decomposition and recursive Bayesian filters

S. Eftekhar Azam, S. Mariani, N.K.A. Attari

Abstract In this paper, an approach based on the synergistic use of proper orthogonal decomposition (POD) and Kalman filtering is proposed for the online health monitoring of damaged structures. The reduced-order model of a structure is obtained during an (offline) initial training stage of monitoring; afterward, effective estimations of a possible structural damage are provided online by tracking the evolution in time of stiffness parameters and projection bases handled in the model order reduction procedure. Such tracking is accomplished via two Kalman filters: a first (extended) one to deal with the time evolution of a joint state vector, gathering the reduced-order state and the stiffness terms degraded by damage; a second one to deal with the update of the reduced-order model in case of damage evolution. Both filters exploit the information conveyed by measurements of the structural response to the external excitations.

Results are reported for a (pseudo-experimental) benchmark test on an eight-story shear building. Capability and performance of the proposed approach are assessed in terms of tracked variation of the stiffness terms of the reduced-order model, identified damage location and speed-up of the whole health monitoring procedure.

Keywords structural health monitoring (SHM); reduced-order modeling; damage detection; model updating; Kalman filtering; proper orthogonal decomposition (POD).

S. Eftekhar Azam

Department of Mechanical Engineering, University of Thessaly, Volos, Greece

S. Mariani (corresponding author)

Department of Civil and Environmental Engineering, Politecnico di Milano, Milan, Italy

E-mail: stefano.mariani@polimi.it

N.K.A. Attari

Structural Engineering Department, Building and Housing Research Center (BHRC), Tehran, Iran

1. Introduction

The rapid growth of infrastructure systems in developing countries has led to the creation of large inventories of structures, featuring new design techniques or new structural systems. Owners got soon aware of the increased safety levels and longevity that can be attained by integrating structural health monitoring (SHM) systems [1]. Further to that, a major portion of infrastructures in developed countries are approaching the foreseen end of their lifecycle [2]; decisions to ensure safety and optimal maintenance strategies, demand once again reliable information on their structural health, see e.g. [3] and [4].

Data related to the structural health have to be collected via a network of (possibly embedded) sensors. As there is no way to directly sense such state of health, data must be interpreted so that meaningful information are extracted from them, see [5]. In recent years, a renewed interest has therefore been focused on various aspects of SHM, including damage detection [6], inspection scheduling and maintenance management [7] and sensor network design [8]. Developments of the sensing method have been provided with surface-mounted MEMS sensors [9,10], fiber Bragg grating sensors [11-13], microwave remote sensing systems [14,15], laser scanning methods [16], GPS measurement systems [17,18] and motion capturing via digital image processing [19-21], to furnish unprecedented dense arrays of data. Accordingly, a need is emerging for an enhancement in signal processing and feature extraction methods, to handle the continuous stream of data provided by the sensors and identify in real-time possible defects.

The detection of a variation in the mechanical properties of structural members or in some features of the measured structural response can be employed as a SHM procedure, see e.g. [22]. If dynamic testing is employed, the aforementioned measured response can be adopted to track the evolution of the structural state from the initial virgin one. Thereafter, the tracked features can be either used for model updating [23-26], or for feeding feature extraction methods and so detecting the location and intensity of a possible damage [27]. If high quality data are available, a detailed assessment of the damage state can be obtained; otherwise, the methods can only detect the existence of damage, see [28]. For additional details on feature extraction in SHM, the interested readers are referred to [29-33].

Since damage processes induce a reduction of stiffness parameters (and therefore a shift in the natural frequencies of the system) [34], linked to a change of geometry or boundary conditions of the structural members or to a degradation of the material properties, damage detection can be viewed as a system identification problem. A number of robust, offline procedures has been developed for the

identification of linear state-space systems: the data driven stochastic subspace identification (SSI) algorithm is the de-facto standard stochastic system identification method for output only scenarios [35,36]; the subspace identification algorithm is instead extensively adopted for the identification of deterministic input-output systems [37,38]. The two aforementioned methodologies include singular value decomposition (SVD) and QR decomposition techniques [39]. To move to online system identification schemes, such methodologies have been modified by focusing on moving time windows of fixed length: as new observations become available, subspace identification is updated. The costs of SVD and QR usually prevent the real-time application of such methods, despite the efforts made to minimize the associated computational burden, see e.g. [37].

In this paper, the focus is on the development of an online damage detection procedure that can be adopted for real-time SHM procedures. The main engine of the proposed method is a recursive Bayesian filter, used to simultaneously estimate the state of the system and the stiffness parameters that can be subjected to a damage-induced degradation. For linear state-space systems disturbed by white Gaussian noises, Kalman filtering is known to provide optimal estimates of the entire state vector upon availability of measurements [40]. By also considering the unknown time-varying stiffness parameters, a nonlinear state-space equation is obtained; the relevant dual identification task has been usually approached via the extended Kalman filter (EKF), which merely relies on a step-by-step linearization of the state-space equations.

In the presence of severe nonlinearities, such linearization was shown to be the cause of instabilities of the filtering procedure, resulting in biases or divergence of the estimates. To deal with severe nonlinearities and general probability distributions of random variables, nonlinear versions of Bayesian filters have been developed, such as the unscented Kalman filter [41] and the particle filter [42]. Both these filters have been then applied to the detection of damage in structures with a relatively low number of degrees-of-freedom (DOFs), see e.g. [43-46]. In this study, a large number of parameters (mostly related to the partially observed structural state) is instead dealt with, and the focus is on a synergy of reduced-order modelling and online system identification. Since an on-the-fly linearized equation of motion is handled, an EKF is adopted for estimation; nonetheless, any nonlinear recursive Bayesian filter could be adopted as well.

If the number of parameters to be estimated (like e.g. the local time-varying stiffness properties in a damaging structure) is small, the above mentioned procedures can provide accurate solutions close to, or in real-time. In [47], it has been shown that, as the number of unknown parameters increases, biases

in the filter estimates show up and increase as well. Within the frame of dual filtering described above, a reduction of the state components looks compulsory and can be obtained with a reduced-order modeling procedure. However, at variance with the identification of the full-order model of the system, the estimated components of the reduced stiffness do not provide an explicit information concerning the intensity and location of damage; so, the identification procedure must be supplemented with additional information coming from the bases adopted to project the full-order governing equations onto the reduced-order (sub)space. The proper orthogonal decomposition (POD) method is here adopted to set the reduced-order model (ROM) of the structural system, so to define the link between the number of DOFs and the accuracy of the ROM on one side, and the needed projector on the other side. If compared to alternative methods, like e.g. an eigenanalysis providing the vibration modes and the relevant frequencies, POD provides some advantages for the online SHM of damaging structures: the ROM is tailored to the specific, structure-dependent loading conditions, and so can lead to a smaller number of DOFs to be dealt with; the ROM has been shown to be (slightly) more accurate than the eigenmode-based one under general loading conditions, see e.g. [60]; the ROM can be experimentally obtained in an initial training stage of the monitoring, prior to any identification of a possible damage state, see the discussion in [45]; through the use of accuracy indices linked to the so-called oriented energy content, see [69], the order of the ROM can be appropriately chosen, and specifically developed algorithms with minimal computational costs can be adopted in the training stage, see e.g. [68]. For a review of the literature related to the application of POD in structural dynamics, see [48].

In [49,50], it was shown that, even in case of highly nonlinear dynamic systems the first two POD modes can accurately capture the evolution of the system. Furthermore, it is known that the POD-based solution is susceptible to a change in case the parameters of the originating model are subject to variations [51]. If POD is adopted to get the ROM, see [52], the mentioned bases, also called proper orthogonal modes (POMs), and the proper orthogonal values (POVs) actually contain information concerning the sought location and intensity of the damage, see e.g. [53-56]; such properties are robustly provided by POD under changing environmental conditions. Taking this feature into account, an algorithm is here proposed for the dual estimation of state and parameters of the reduced-order model with an EKF, wherein the damage-dependent POMs are continuously updated by a further Kalman filter without the need of time consuming re-training stages. A synergy of the two recursive Bayesian filters and of POD is exploited in a decoupled two-stage procedure: first, the joint filtering scheme is adopted to obtain estimates of the stiffness parameters relevant to the ROM; second, the

linear correlation between the subspace spanned by POMs and the observation equation is exploited for model updating purposes.

The remainder of this paper is organized as follows. In Section 2, details are provided on the reduced-order modeling technique through POD and on the resulting state-space model; since model parameters (i.e. stiffness properties of the structure) are to be estimated, it is shown how the state vector has to be augmented and how the resulting observation equation, that has to link the reduced-order state with the observables of the full-order one, needs to be modified accordingly; the sensitivity to damage of features of the POD-based ROM is also addressed. Section 3 deals with the implementational details of the concurrent dual estimation of the ROM, and update of the ROM itself due to damage evolution (if any); some details are also provided concerning the expected (so-called asymptotic) speed-up in the analysis, as furnished by the computational complexity of all the algorithmic stages. In Section 4, the capability and performance of the proposed approach are discussed with reference to a shear building. Finally, Section 5 collects some concluding remarks on the proposed procedure, and also possible strategies to extend its applicability to complex, real-life structures.

2. Reduced-order state-space model of partially observed dynamic systems

Let us consider a space-discretized structural system. If $\boldsymbol{u}$, $\dot{\boldsymbol{u}}$ and $\ddot{\boldsymbol{u}}$ respectively represent the relevant displacement, velocity and acceleration vectors that all belong to $\mathbb{R}^m$, where m is the number of DOFs of the full-order model, the (vectorial) equation of motion of the system reads:

$$\boldsymbol{M}\ddot{\boldsymbol{u}} + \boldsymbol{D}\dot{\boldsymbol{u}} + \boldsymbol{K}(t)\boldsymbol{u} = \boldsymbol{f}(t) \tag{1}$$

where: $\boldsymbol{M}$, $\boldsymbol{D}$ and $\boldsymbol{K}$ are the mass, viscous damping and stiffness matrices belonging to $\mathbb{R}^{m\times m}$, respectively; and $\boldsymbol{f} \in \mathbb{R}^m$ is the time-varying loading vector. In Eq. (1) we have assumed the mass and damping matrices to be time-invariant, whereas the stiffness properties can evolve in time due to possible damage phenomena. The term $\boldsymbol{K}(t)\boldsymbol{u}$ can be alternatively considered as the internal force vector $\boldsymbol{f_i}(t) \in \mathbb{R}^m$, which is therefore linked to the current mechanical properties of the structure. Here, as we do not focus on numerical procedures to model damage and, therefore, stiffness evolution, we have explicitly highlighted the stiffness matrix $\boldsymbol{K}$ in Eq. (1), and assumed it to be a function of time t. For further details readers are referred to [57], where a thorough analysis was reported on the identification of a damaging structure.

In system identification and, specifically, in SHM procedures, the properties in matrices $\boldsymbol{M}$, $\boldsymbol{D}$ and $\boldsymbol{K}$, or at least estimations of them, are supposed to be available. Even if such structural properties are

affected by uncertainties not explicitly considered in the design phase, the procedure to be proposed next for the setting of the ROM can be supported by an identification scheme that finely tunes the said full-order matrices; this additional task, not addressed here but already envisaged in [45], can then allow to study damage evolution in systems affected by initial uncertainties in their physical properties. Within the stochastic framework for system identification to be provided in Section 3, such uncertainties in the stiffness matrix $\boldsymbol{K}$ are actually accounted for through ad-hoc formulated process/model errors.

By partitioning the time interval of interest according to $[t_0 \ t_N] = \cup_{k=1}^{N}[t_{k-1} \ t_k]$, and by adopting a standard Newmark explicit integrator to advance the solution of Eq. (1) in time, a state-space form of the fully discretized equation of motion is obtained as:

$$\boldsymbol{z}_k = \boldsymbol{A}_k \, \boldsymbol{z}_{k-1} + \boldsymbol{b}_k \tag{2}$$

where $\boldsymbol{z}_k \in \mathbb{R}^{3m}$ is the state vector for the system, which gathers all the displacements, velocities and accelerations according to:

$$\boldsymbol{z}_k = \begin{Bmatrix} \boldsymbol{u}_k \\ \dot{\boldsymbol{u}}_k \\ \ddot{\boldsymbol{u}}_k \end{Bmatrix} \tag{3}$$

and the algorithmic mapping matrix $\boldsymbol{A}_k \in \mathbb{R}^{3m\times 3m}$ and vector $\boldsymbol{b}_k \in \mathbb{R}^{3m}$ respectively read:

$$\boldsymbol{A}_k = \begin{bmatrix} \boldsymbol{I} - \beta\,\Delta t^2 \boldsymbol{K}_k\,\boldsymbol{M}^{-1} & \Delta t\,\boldsymbol{I} - \beta\,\Delta t^2 \boldsymbol{M}^{-1}(\boldsymbol{D} + \Delta t\,\boldsymbol{K}_k) & -\beta\,\Delta t^2 \boldsymbol{M}^{-1}\left(\Delta t^2\left({}^1/_2 - \beta\right)\boldsymbol{K}_k + \Delta t(1-\gamma)\,\boldsymbol{D}\right) + \Delta t^2\left({}^1/_2 - \beta\right)\boldsymbol{I} \\ -\gamma\,\Delta t\,\boldsymbol{K}_k\boldsymbol{M}^{-1} & \boldsymbol{I} - \gamma\,\Delta t\boldsymbol{M}^{-1}(\boldsymbol{D} + \Delta t\,\boldsymbol{K}_k) & -\gamma\,\Delta t\boldsymbol{M}^{-1}\left(\Delta t^2\left({}^1/_2 - \beta\right)\boldsymbol{K}_k + \Delta t(1-\gamma)\,\boldsymbol{D}\right) + \Delta t(1-\gamma)\,\boldsymbol{I} \\ -\boldsymbol{K}_k\boldsymbol{M}^{-1} & -\boldsymbol{M}^{-1}(\boldsymbol{D} + \Delta t\,\boldsymbol{K}_k) & -\boldsymbol{M}^{-1}\left(\Delta t^2\left({}^1/_2 - \beta\right)\boldsymbol{K}_k + \Delta t(1-\gamma)\,\boldsymbol{D}\right) \end{bmatrix} \tag{4}$$

$$\boldsymbol{b}_k = \begin{Bmatrix} \beta\,\Delta t^2 \boldsymbol{M}^{-1}\,\boldsymbol{f}_k \\ \gamma\,\Delta t\,\boldsymbol{M}^{-1}\boldsymbol{f}_k \\ \boldsymbol{M}^{-1}\boldsymbol{f}_k \end{Bmatrix} \tag{5}$$

β and γ being the Newmark parameters, see e.g. [58]. In these equations: a subscript k means that the relevant variable is computed at time instant t_k (the same holds for index $k-1$ and instant t_{k-1}); $\Delta t = t_k - t_{k-1}$ is the time step size, here assumed constant during the whole analysis; and $\boldsymbol{I}$ is the identity matrix.

SHM requires the system to be at least partially observed. Accordingly, in a deterministic frame the observation equation at time t_k reads:

$$\boldsymbol{y}_k = \boldsymbol{H}\boldsymbol{z}_k \tag{6}$$

where: $\boldsymbol{y}_k \in \mathbb{R}^n$ is the vector of the n observables; and $\boldsymbol{H} \in \mathbb{R}^{n\times 3m}$ is a Boolean matrix of appropriate dimensions, which links the state $\boldsymbol{z}_k$ of the system to the observations in $\boldsymbol{y}_k$. As the monitoring system

collects information on the structural health through sensor measurements, a time-independent matrix $\boldsymbol{H}$ means that the type of sensors adopted and their deployment over the structure are never changed.

Due to the definition (3) of the state vector $\boldsymbol{z}_k$, whose dimension is three times the number m of DOFs of the discrete system, any identification procedure based on the adopted state-space model gives rise to a considerable computational burden. Anyhow, as thoroughly discussed in [59], [57] and [45], this state-space representation is necessary whenever the nonlinear evolution of the structural system (due to, e.g. damage growth) is studied within a stochastic framework: if all the state variables were not listed in $\boldsymbol{z}_k$, part of the information concerning the step-by-step evolution of the statistics of the state would be missed.

2.1. Reduced-order modelling via POD

To reduce the computational burden, keeping a high accuracy of the numerical model as a target, POD is next exploited. It is well recognized that POD provides a model-specific and, somehow, also load-specific optimal linear subspace, onto which the system dynamics can be projected. This subspace is not supposed to evolve in time, once obtained at the end of an initial training stage of the analysis, see e.g. [60].

To deal with structural systems undergoing damage evolution and therefore requiring an update of the subspace itself, the training stage is typically repeated whenever the reduced-order model is no more able to provide an accurate input-output relation, see [68]. To avoid the computational costs of repeated training stages, an adaptive procedure governed by a Kalman filter will be reported in the forthcoming Section 3.

We now discuss the main technical details of the POD-based reduced-order modeling technique, to also highlight the role of the observation equation in the aforementioned adaptive procedure. For linear systems, the displacement field can be written in a separable form as:

$$\boldsymbol{u}(\boldsymbol{x},t) = \sum_{i=1}^{m} \boldsymbol{\varphi}_i(x)\alpha_i(t) \tag{7}$$

where: vectors $\boldsymbol{\varphi}_i(x)$ belong to a set of arbitrary bases spanning $\mathbb{R}^m$, called proper orthogonal modes (POMs); and coefficients α_i define the time-varying amplification of such bases. While the system is moving due to the external excitation, a "structure" in the response (linked in some sense to the vibration modes, see e.g. [69]) usually reduces considerably the number of effective terms in Eq. (7). So, if the main variation in the data occurs in a rather small subspace of $\mathbb{R}^m$, it is possible to track the evolution of the system by keeping only l terms in the expansion of Eq. (7), with $l \ll m$. Accordingly:

$$\boldsymbol{u}(\boldsymbol{x},t) \approx \sum_{i=1}^{l} \boldsymbol{\varphi}_i(x)\alpha_i(t) = \boldsymbol{\Phi}_l\,\boldsymbol{\alpha} \tag{8}$$

where: the matrix $\boldsymbol{\Phi}_l \in \mathbb{R}^{m\times l}$ gathers (as columns) the l POMs retained in the ROM; and vector $\boldsymbol{\alpha}$ provides the time evolution of the POMs, and so it gathers the DOFs of the model. By substituting Eq. (8) into (1), by defining a residual vector linked to the approximation (8), and by eventually adopting a Galerkin projection onto the same reduced-order subspace adopted in (8), the equation of motion of the system can be written:

$$\boldsymbol{\mathcal{M}}\ddot{\boldsymbol{\alpha}} + \boldsymbol{\mathcal{D}}\dot{\boldsymbol{\alpha}} + \boldsymbol{\mathcal{K}}\boldsymbol{\alpha} = \boldsymbol{\mathcal{f}}(t) \tag{9}$$

where:

$$\boldsymbol{\mathcal{M}} = \boldsymbol{\Phi_l}^{\mathrm{T}}\boldsymbol{M}\boldsymbol{\Phi_l}, \quad \boldsymbol{\mathcal{D}} = \boldsymbol{\Phi_l}^{\mathrm{T}}\boldsymbol{D}\boldsymbol{\Phi_l}, \quad \boldsymbol{\mathcal{K}} = \boldsymbol{\Phi_l}^{\mathrm{T}}\boldsymbol{K}\boldsymbol{\Phi_l}, \quad \boldsymbol{\mathcal{f}} = \boldsymbol{\Phi_l}^{\mathrm{T}}\boldsymbol{f} \tag{10}$$

To set the accuracy of the reduced-order model and define the number l of POMs to be retained, the error linked to the approximation (8) needs to be quantified. According to the snapshot version of POD [70], during the initial stage of the analysis snapshots of nodal displacements $\boldsymbol{u}_j = \boldsymbol{u}(t_j)$ at time instants t_j, $j = 1, \dots, J$, are collected in the so-called snapshot matrix $\boldsymbol{U} \in \mathbb{R}^{m\times J}$. A singular value decomposition of matrix $\boldsymbol{U}$ then provides:

$$\boldsymbol{U} = \boldsymbol{L}\boldsymbol{\Lambda}\boldsymbol{R}^{\mathrm{T}} \tag{11}$$

where: $\boldsymbol{L} \in \mathbb{R}^{m\times m}$ and $\boldsymbol{R} \in \mathbb{R}^{J\times J}$ are, respectively, the matrices gathering the left and right orthonormal singular vectors; $\boldsymbol{\Lambda} \in \mathbb{R}^{m\times J}$ is the pseudo-diagonal matrix, whose pivotal entries Λ_{ii} are the singular values of $\boldsymbol{U}$. As proved in [71], $\boldsymbol{L}$ collects all the POMs and, if singular values Λ_{ii} are sorted decreasingly, l can be set by assigning:

$$\frac{\sum_{i=1}^{l}\Lambda_{ii}^2}{\sum_{i=1}^{m}\Lambda_{ii}^2} \geq p \tag{12}$$

where $p \in (0\ \ 1]$ is an accuracy index based on the energy content of the ROM. It should be noted that the main priority in this study is not the development of a very accurate ROM of the system, but instead the setting of a very compact model with a minimal number of parameters to be estimated in real-time. It is expected that part of the model inaccuracy can be handled and compensated for by the recursive Bayesian filters employed herein for system identification.

Even though POD is optimal for linear systems only, it can be applied to model order reduction of nonlinear systems too, see [61-64]. A number of authors have studied the links between POMs and linear normal modes of structural systems, showing that in case of free undamped oscillations the POMs converge to the linear normal modes for a sufficiently large number of collected samples or

snapshots [65,66]. The POVs have been also used as indicators of modal activity, and it was shown that they can accurately determine the number of active modes in the dynamic response of a structure [67].

2.2. State-space representation of the ROM

Similarly to what reported for the full-order model, the reduced-order state-space form of system evolution in the time step $[t_{k-1}\ \ t_k]$ can now be written as:

$$\boldsymbol{\zeta}_k = \boldsymbol{\mathcal{A}}_k \boldsymbol{\zeta}_{k-1} + \boldsymbol{\mathscr{b}}_k + \boldsymbol{v}_k^{\zeta} \tag{13}$$

$$\boldsymbol{y}_k = \boldsymbol{H}\, \boldsymbol{\mathcal{C}}\, \boldsymbol{\zeta}_k + \boldsymbol{v}_k^{y} \tag{14}$$

where the state vector $\boldsymbol{\zeta}_k \in \mathbb{R}^{3l}$ collects the retained DOFs and their time derivatives, according to:

$$\boldsymbol{\zeta}_k = \begin{Bmatrix} \boldsymbol{\alpha}_k \\ \dot{\boldsymbol{\alpha}}_k \\ \ddot{\boldsymbol{\alpha}}_k \end{Bmatrix} \tag{15}$$

and:

$$\boldsymbol{\mathcal{C}} = \begin{bmatrix} \boldsymbol{\Phi}_l & & \\ & \boldsymbol{\Phi}_l & \\ & & \boldsymbol{\Phi}_l \end{bmatrix} \tag{16}$$

$\boldsymbol{\mathcal{C}} \in \mathbb{R}^{3m \times 3l}$ is a matrix introduced to deal with the observation equation (6), and so to move from the reduced-order space to the full-order one while sorting out the system DOFs actually observed. Matrix $\boldsymbol{\mathcal{A}}_k \in \mathbb{R}^{3l}$ and vector $\boldsymbol{\mathscr{b}}_k \in \mathbb{R}^{3l \times 3l}$ are not reported here for brevity, as they can be obtained from Eqs. (4) and (5) simply by switching from the full-order properties $\boldsymbol{M}, \boldsymbol{D}, \boldsymbol{K}_k, \boldsymbol{f}_k$ to the reduced-order ones $\boldsymbol{\mathcal{M}} \in \mathbb{R}^{l \times l}, \boldsymbol{\mathcal{D}} \in \mathbb{R}^{l \times l}, \boldsymbol{\mathcal{K}}_k \in \mathbb{R}^{l \times l}, \boldsymbol{\mathscr{f}}_k \in \mathbb{R}^{l}$, see Eq. (10).

As real systems evolve in a noisy environment, they are affected by uncertainties. Accordingly, Eqs. (13) and (14) have been provided with additive terms $\boldsymbol{v}_k^{\zeta}$ and $\boldsymbol{v}_k^{y}$ respectively representing the time-varying process and measurement noises. In what developed here above, it is worth noting that the process noise also stems from the loss of accuracy of the ROM, as stated in Eq. (12) where it is typically set $p < 1$ for reasons linked to the computational costs.

Each noise source is usually assumed to be white and uncorrelated in time; this assumption largely simplifies the analysis, since only the relevant mean and covariance terms need to be handled. In case of a colored noise, it is necessary to determine the structure of correlations in the noise sequence and auto regressive (AR) models of some order, say n_{AR}, are used to capture such dependencies. The noise process at time t_k can be then rewritten as a linear combination of a white noise $\boldsymbol{\varepsilon}_k^{\zeta}$ and of the noise

terms at the n_{AR} preceding time steps, according to $\boldsymbol{v}_k^{\zeta} = \sum_{i=1}^{n_{\mathrm{AR}}} \tau_i \boldsymbol{v}_{k-i}^{\zeta} + \boldsymbol{\varepsilon}_k^{\zeta}$, where τ_i are the AR coefficients. Dealing with colored noise processes, the process itself is commonly added to the state vector and the state-space formulation is appropriately reformulated, see [72]; in some cases, an AR model may not be adequate and an auto regressive moving average (ARMA) model is required to extract the correlations in the noise signals, see [73]. In [47], a detailed statistical investigation was reported for errors linked to the formulation of POD-based ROMs; as the accuracy of such models gets higher close to the POM frequencies, the residual error due to POD (which is part of $\boldsymbol{v}_k^{\zeta}$) turns out to be far from being white. Anyhow, by increasing the number of POMs retained in the analysis, a consistent reduction of the amplitude of the noise signal and of its spectral power was reported. Therefore, to systematically avoid issues related to colored noise the number of POMs can be increased without making recourse to ARMA models, which inherently increase the dimension of the state vector and act against reducing the order of the model. As the emphasis of this paper is on how to deal with the curse of dimensionality, which shows up if the number of model DOFs get increased, inaccuracies caused by colored noise are neglected even if a suboptimal performance of the filter to be introduced next is expected. The effects of uncertainties in Eqs. (13) and (14) are thus handled as in any standard recursive Bayesian inference algorithm, see [74].

In the stochastic framework defined above, stiffness parameters can be assumed affected by uncertainties due to imperfections, or incepted damage processes. By estimating their evolution during the analysis, the monitoring system is able to provide a forecast of the developed damage pattern. Model parameters to be identified are so collected in a vector $\boldsymbol{\vartheta} \in \mathbb{R}^{N_p}$, to be considered as material- or structure-dependent. Fluctuations of this vector are thus allowed for to improve the estimates or to identify the evolution of damage leading to a reduction of the structural stiffness, moving from an initial guess at time t_0. To cope with both these goals, the vector is assumed to evolve according to a random walk:

$$\boldsymbol{\vartheta}_k = \boldsymbol{\vartheta}_{k-1} + \boldsymbol{v}_k^{\vartheta} \tag{17}$$

where $\boldsymbol{v}_k^{\vartheta}$ is an additional white and uncorrelated artificial noise.

In the forthcoming numerical examples, we consider the mass properties of the structure to be known with a high level of fidelity. Furthermore, the structural response is supposed to be monitored in the special case of known damping; the effect of damping on filtering in dynamics was already considered in [59], and is not further discussed here. Therefore, all the terms of matrices $\boldsymbol{\mathcal{M}}$ and $\boldsymbol{\mathcal{D}}$ are not to be

identified and included in the vector $\boldsymbol{\vartheta}$; parameters to tune are only the entries of the stiffness matrix $\boldsymbol{\mathcal{K}}$. It is also to be noted that model-order reduction can detrimentally affect the capability of identifying the exact location and amount of damage. In fact, by projecting the stiffness matrix over the subspace of the retained POMs according to $\boldsymbol{\mathcal{K}} = \boldsymbol{\Phi_l}^{\mathrm{T}} \boldsymbol{K} \boldsymbol{\Phi_l}$, see Eq. (10), different damage mechanisms can become correlated; in other words, a single POM can excite simultaneously different damaged zones of the structure, and the estimated evolution of the entries of $\boldsymbol{\vartheta}_k$ would be a smeared measure of the structural damage. Anyhow, as shown in the results Section, the shape of POMs provides additional, helpful information concerning the location of possible multiple damage sites.

To deal with the dual estimation problem, see e.g. [75], we now augment the state vector of the ROM, so that at time t_k it reads:

$$\boldsymbol{\chi}_k = \begin{Bmatrix} \boldsymbol{\zeta}_k \\ \boldsymbol{\vartheta}_k \end{Bmatrix} \tag{18}$$

By joining together state and model parameters in the vector $\boldsymbol{\chi}_k \in \mathbb{R}^{3l+N_p}$, the state-space equations become nonlinear. We therefore formulate the system evolution equations as:

$$\boldsymbol{\chi}_k = \boldsymbol{\psi}_k(\boldsymbol{\chi}_{k-1}) + \boldsymbol{v}_k^{\chi} \tag{19}$$

$$\boldsymbol{y}_k = \boldsymbol{H}\, \boldsymbol{\mathcal{L}}\, \boldsymbol{\chi}_k + \boldsymbol{v}_k^{y} \tag{20}$$

where matrix $\boldsymbol{\mathcal{L}} \in \mathbb{R}^{3m \times (3l+N_p)}$ reads:

$$\boldsymbol{\mathcal{L}} = [\boldsymbol{\mathcal{C}} \quad \boldsymbol{0}] \tag{21}$$

and links the reduced-order augmented state of the system to the full-order one. Furthermore: function $\boldsymbol{\psi}_k \in \mathbb{R}^{3l+N_p}$ maps the augmented state of the system in time; and $\boldsymbol{v}_k^{\chi}$ is the state error, that accounts for both the contributions $\boldsymbol{v}_k^{\zeta}$ and $\boldsymbol{v}_k^{\vartheta}$ introduced before. Errors $\boldsymbol{v}_k^{\chi}$ and $\boldsymbol{v}_k^{y}$ are still assumed as zero mean white Gaussian processes, featuring time-invariant covariance matrices $\boldsymbol{V}^{\chi}$ and $\boldsymbol{V}^{y}$.

In Section 3 an extended Kalman filter will be proposed to handle the state-space model (19)-(20), so as to simultaneously track the state $\boldsymbol{\zeta}_k$ and calibrate the parameters in $\boldsymbol{\vartheta}_k$. In case of damage evolution leading to a drift of the structural response, a further Kalman filter is adopted to tune on-the-fly the retained POMs, and so matrix $\boldsymbol{\Phi_l}$ affecting $\boldsymbol{\mathcal{L}}$.

2.3. Sensitivity of POMs to damage events

In vibration-based SHM methods it is assumed that damage may cause changes in the stiffness, damping and sometimes mass properties of the system; therefore, it can also modify the vibration characteristics of the structure. The sensitivity of POMs to damage has been exploited by several

authors, see e.g. [55,56]. Galvanetto and Violaris showed that POMs can be used to detect and locate damage in beam-type structures [55]: they plotted the POMs of the reference (undamaged) structure versus those of the damaged one, and concluded that the difference between the two can be used to identify damage location and severity. Shane and Jha developed an offline algorithm for damage identification in composite beams [56]: adopting a finite element model of the composite beam, different damage scenarios were created featuring varying degrees of stiffness reduction. Their algorithm, which took advantage of POMs as dynamic invariants of the structure, was successfully used to identify damage even under changing loading and environmental conditions.

It is thus clear that POMs can potentially be used for quantifying damage in structures. In contrast to former works, the focus of the current study is on the development of an algorithm for the online and real-time update of POMs and relevant parameters of the POD-based ROM of a damaging structural system, so as damage quantification and location can be automatically (or semi-automatically) obtained as a byproduct.

3. Concurrent dual estimation of the reduced-order model and model updating

As already pointed out, the dual estimation problem here envisioned consists, at time t_k, in the estimation of the whole reduced-order state $\boldsymbol{\chi}_k$ of the system, including the stiffness parameters collected in $\boldsymbol{\vartheta}_k$.

For a non-damaging structure, such dual estimation can be pursued without any update of the ROM as it never changes; hence, matrix $\boldsymbol{\Phi}_l$ is calibrated in the initial training stage of the analysis, and handled as is along the whole SHM stage. On the contrary, the projection matrix $\boldsymbol{\Phi}_l$ of a damaging structure varies in time due to a possibly non-uniform reduction of the stiffness characteristics, causing a change of the POMs. As a consequence, to avoid the state estimates to be affected by drifts in time, the aforementioned dual estimation procedure must be backed by an online update of the projection subspace, i.e. of all the retained POMs.

We propose now an approach for the online subspace update, and simultaneous estimation of the partially observed state of the system and of model parameters affected by uncertainties. In order to accomplish these tasks online, the adopted engines are two Bayesian filters: an extended Kalman filter handles the dual estimation task, which turns out to be nonlinear (actually, bilinear) due to the joint estimation of terms in $\boldsymbol{\mathcal{A}}_k$ and $\boldsymbol{\zeta}_k$ in Eq. (13), as summarized by mapping $\boldsymbol{\psi}_k$ in Eq. (19); a Kalman filter handles instead the subspace update for the ROM.

To allow for the time variation of the model subspace, retained POMs (see Eq. 8) are now arranged in vector form as:

$$\boldsymbol{\Xi}_{l,k} = \begin{Bmatrix} \boldsymbol{\varphi}_{1,k} \\ \vdots \\ \boldsymbol{\varphi}_{l,k} \end{Bmatrix} \tag{22}$$

where $\boldsymbol{\Xi}_{l,k} \in \mathbb{R}^{ml}$ and the index k has been added to explicitly state that POMs can vary in time. Accounting for the stochastic environment within which the system evolves, the projection subspace evolution is described by:

$$\boldsymbol{\Xi}_{l,k} = \boldsymbol{\Xi}_{l,k-1} + \boldsymbol{v}_k^{\varphi} \tag{23}$$

where $\boldsymbol{v}_k^{\varphi}$ is a fictitious zero mean white Gaussian noise, whose time-invariant covariance $\boldsymbol{V}^{\varphi}$ needs to be tuned to get unbiased estimates of the POMs, and so of model parameters to be identified.

Eq. (23) has now to be supplemented by an observation equation, to drive the update of $\boldsymbol{\Xi}_{l,k}$ through the acquired measurements in $\boldsymbol{y}_k$. For this purpose, Eq. (20) is written in a slightly rearranged version so as to explicitly highlight the role of POMs. Within the current time step, by assuming the state $\boldsymbol{\chi}_k$ to be independent of the subspace adopted, the following relation is arrived at:

$$\boldsymbol{y}_k = \boldsymbol{\mathcal{H}}\boldsymbol{\Xi}_{l,k} + \boldsymbol{v}_k^{y} \tag{24}$$

where $\boldsymbol{\mathcal{H}} \in \mathbb{R}^{n \times ml}$ is the mapping that links the observations to the subspace spanned by POMs. The two Eqs. (23) and (24) provides now the state-space model for subspace evolution: due to its linearity, a Kalman filter, which is the optimal estimator for linear state-space models, is then adopted for the recursive update of the subspace.

Table 1 provides the algorithmic description of the proposed procedure. As any Bayesian filtering scheme, the algorithm consists in the initialization of the solution at time t_0, and the evolution of it at all the subsequent discrete time instants t_k, up to t_N. In turn, the evolution of the estimates is subdivided into two stages: a prediction one, which rests on the mapping equations (19) and (23) to evolve the expected values of augmented state and subspace, and the relevant covariances; an update one, which is driven by the Kalman gains $\boldsymbol{G}_{\chi,k} \in \mathbb{R}^{(3l+N_p)\times n}$ and $\boldsymbol{G}_{\varphi,k} \in \mathbb{R}^{ml \times n}$ to account for the information provided by measurements. Besides what is already defined above, here: $\boldsymbol{\mathcal{F}}_k = \left.\frac{\partial \boldsymbol{\psi}_k(\boldsymbol{\chi})}{\partial \boldsymbol{\chi}}\right|_{\boldsymbol{\chi}=\hat{\boldsymbol{\chi}}_{k-1}}$ is the Jacobian of the reduced-order state mapping $\boldsymbol{\psi}_k$, computed with the state estimation $\hat{\boldsymbol{\chi}}_{k-1}$ available at the beginning of the time step; the superposed hat denotes the estimated values of augmented state and POMs, provided by the filtering scheme; the covariance terms for state

and subspace are respectively defined as $\boldsymbol{\mathcal{P}}_k = \mathbb{E}[(\boldsymbol{\chi}_k - \widehat{\boldsymbol{\chi}}_k)(\boldsymbol{\chi}_k - \widehat{\boldsymbol{\chi}}_k)^{\mathrm{T}}]$ and $\boldsymbol{\Pi}_k = \mathbb{E}\left[\left(\boldsymbol{\Xi}_{l,k} - \widehat{\boldsymbol{\Xi}}_{l,k}\right)\left(\boldsymbol{\Xi}_{l,k} - \widehat{\boldsymbol{\Xi}}_{l,k}\right)^{\mathrm{T}}\right]$, where $\mathbb{E}$ is the expectation operator; gains $\boldsymbol{G}_{\chi,k}$ and $\boldsymbol{G}_{\varphi,k}$ respectively drive the update of $\widehat{\boldsymbol{\chi}}_k$ and $\widehat{\boldsymbol{\Xi}}_{l,k}$; matrix $\boldsymbol{\mathcal{L}}$ becomes time-dependent too, since POMs in $\boldsymbol{\Xi}_{l,k}$ vary in time. A summary of the whole procedure is reported in Figure 1, where a possible post-processing phase has been also added in case a specific feature extraction step looks necessary to finely identify the damage state.

As already reported in [76] for a different approach, wherein damage indices (each one assumed constant inside a sub-domain of the discretized structure) were included into the augmented state vector in place of the reduced-order stiffness terms here handled, the main advantage of the splitting of $\boldsymbol{\chi}_k$ and $\boldsymbol{\Xi}_{l,k}$ reported in Table 1, in comparison with other methods conventionally used for model updating (see, e.g. [77]), is that the linearity of the state-space subspace model of Eqs. (23) and (24) is explicitly exploited. For the online estimation of POMs, the Kalman filter therefore provides a closed-form, optimal solution to the problem. A problem may anyway arise as the observation equation and the relevant innovation term in the update stage, although written in the two slightly different ways $\boldsymbol{y}_k - \boldsymbol{H}\boldsymbol{\mathcal{L}}_k\boldsymbol{\chi}_k^-$ and $\boldsymbol{y}_k - \boldsymbol{\mathcal{H}}\boldsymbol{\Xi}_{l,k}^-$ for the reasons discussed here above, are accounted for twice within a single time step. It is therefore supposed that a certain degree of redundancy in the set of measurements would help avoid biases in the estimates, or the generally reported filter instability, see [78]. At any rate, a thorough discussion on the conditions (in terms, e.g. of sensor deployment and accuracy) to be attained to guarantee the convergence of POMs towards a steady-state solution in case of no further damage evolution, is out of the scopes of this paper and left for future investigations.

To assess the analysis speed-up or gain provided by moving from the full-order model to the ROM, a note on the computational complexity of the algorithmic prediction-update process of Table 1 is discussed next. Within each time step, the aforementioned computational complexity is provided in terms of the order of the required floating-point operations. Concerning the reduced-order modeling, as training is carried out once and in an offline manner, the complexity associated with it is not included in the assessment; Table 2 then summarizes the complexities of all the stages in Table 1. The prediction of the state scales quadratically with its dimension $3l + N_p$, whereas the prediction of its covariance scales cubically with the same dimension. The prediction of the subspace and of its covariance scales instead quadratically with the dimension ml of $\boldsymbol{\Xi}_{l,k}$. As for the update stage, in the computation of the two Kalman gains a square $n \times n$ matrix must be inverted, and the related computational complexity

is $O(n^3)$ if a standard Gauss-Jordan procedure is adopted [79]. Concerning the $\boldsymbol{\mathcal{H}}$ matrix, the complexity associated with its calculation is $O(lmn)$. In the update of POMs, the procedure also includes a normalization of the subspace estimates, whose complexity is $O(lm)$; however, the complexity of this stage is dominated by the other matrix operations. Overall, the computational complexity of the whole procedure at time t_k turns out to be:

$$O\left(n^3 + n\left(3l + N_p\right)^2 + n^2\left(3l + N_p\right) + n\left(3n + 3m + N_p\right)\left(3l + N_p\right) + lmn^2 \ + n(lm)^2 + \left(3l + N_p\right)^3\right) \tag{25}$$

If the full-order model is used within the same framework, the relevant numerical complexity will instead read:

$$O\left(\left(N_p + 3m\right)^3 + n\left(N_p + 3m\right)^2 + n^2\left(N_p + 3m\right) + n^3\right) \tag{26}$$

where account has been taken that POMs do not have to be estimated and updated in time.

As already discussed in [75], an estimate of the analysis speed-up provided by reduced-order modeling can be given as the ratio between the computational complexities furnished by Eqs. (26) and (25); such estimate will be adopted in Section 4 to discuss the performance of the proposed procedure. The complexities discussed here above anyway refer to asymptotic scenarios; the real CPU times and the corresponding speed-ups could be different from them due to, e.g. processor architecture, hardware settings, and structure of the matrices.

It must be finally noted that, within a deterministic setup even small variations of the structural health can lead to detectable changes in the measurable structural response $\boldsymbol{y}_k$ to loadings. In real situations, various sources of uncertainty linked to the measurements, to the excitation and to the structural properties in the initial state can all lead to significant scattering in the estimates of modal parameters; consequently, only the effects of significant levels of damage could be observed and detected. The currently proposed intricate Bayesian framework for the online and real-time update of a ROM of the structural system is aimed at mitigating the aforementioned issues related to modelling errors and observation noises, due to the concurrent use of two Kalman filters that provide estimates of the whole state. Accordingly, the proposed approach is expected to be more robust, and to allow detection of small levels of damage independently of the structural scheme.

4. Numerical results: damage detection in an eight-story shear building

To assess the capability of the proposed approach, the benchmark problem proposed in [80] is now considered. An eight-story shear building features constant floor mass of 625 ton, and inter-story stiffness of 10^6 kN/m; as the problem of nonclassical damping is not addressed here, at variance with what reported in [80] a Rayleigh damping with damping ratio of 2% for the first two structural modes has been assumed. Concerning the possible detrimental effects of damping on the identifiability of dynamic systems, a discussion was already reported in [59]; overall, it was claimed that, if the structure is continuously excited, damping has only marginal effects in this regard. Loading is provided by a force applied to the last floor of the building and varying sinusoidally for the entire duration of monitoring, according to $f(t) = 5 \cdot 10^6 \sin \pi t$ N.

Pseudo-experimental data have been created by running a direct analysis, sampling the target structural output (in terms of story displacements) every 0.01 s and then corrupting it with uncorrelated zero mean, white Gaussian noises featuring a standard variation 0.0032 m to allow for the uncertainties in measurements.

4.1. Pre-processing of the baseline model and damage-sensitive features

Focusing first on the outcome of the training stage of POD, Figure 2 provides the shape of the retained POM for $l = 1$, both for the undamaged structure and when damage of a varying intensity d is located only between the fourth and fifth floors. The scalar damage variable d has to be intended as in standard damage mechanics, see [81], so scaling the inter-story stiffness terms according to $K_{ij}^d = (1 - d)K_{ij}$, where K_{ij} is the virgin value and K_{ij}^d is the corresponding damaged one, and ij are the indices relevant to the two adjacent storys. This definition of the dependence on damage of the properties of the full-order model means that only the terms related to a specific inter-story stiffness are affected, while all the others are not varied. We do not consider here the simultaneous presence of multiple damage states at different storys, so no ambiguity results from what reported here above; alternatively, a different damage index would be defined for each inter-story stiffness term.

The plots in Figure 2 clearly show that a kink shows up only at the inter-story affected by a reduction of the stiffness. Similar results, showing kinks in the POMs where a damage or a crack is located, were already reported e.g. in [64] for beams. This feature would be of help if training of the ROM were continuously carried out after the inception of damage, as it immediately allows locating it and also estimating its intensity on the basis of the local change in slope. As such time consuming approach is

purposely avoided within the proposed framework, the output of the SHM procedure needs to be post-processed to get insights into the damage state, see also below. Results of Figure 2 can be easily extended to allow for a damage located at different floors: plots of relevant POM shapes are reported in Figure 3 for the exemplary case $d = 0.5$.

If $l = 2$, Figure 4 provides the shapes of both POMs, still in the undamaged case and when $d = 0.5$ at the inter-story between the fourth and fifth floors. Although the shape of POM #1 obtained with the two ROMs (featuring orders $l = 1$ and $l = 2$) look the same, the model is not necessarily order-invariant as the projectors onto the two different subspaces are different. A thorough discussion on the relationship between POMs and vibration modes in the linear regime was proposed in [69]: for multi-DOF systems, it was shown that training provides POMs converging towards the eigenmodes at resonance. For the considered excitation mentioned above, resonance does not occur and so it can be only claimed that POMs and eigenmodes are similar, with the former ones also varying with l, and they can bring similar information concerning the damage location. In fact, the graphs show that damage gives rise to kinks in both the damaged POMs, accompanied by a local amplification of the relative story displacements.

As far as the overall accuracy of the two ROMs featuring $l = 1$ and $l = 2$ is concerned, Table 3 gathers the relevant values of index p (see Eq. 12) for the undamaged and damaged states, the first one as given at the end of training and the second one computed (to be reported here even if not handled in the proposed procedure) when a steady-state solution is attained by the identified entries of the reduced-order stiffness matrix. It is shown that, due to the system geometry and loading conditions, one POM proves sufficient to obtain an extremely high energetic accuracy, which is indeed not detrimentally affected by damage.

Although this issue is not to be discussed here in details, before the SHM procedure based on the ROM is started one needs to ensure that all the POMs has already attained a stationary solution, and so training has been completely accomplished (typically, for the initial damage-free state). Two alternate proposals were discussed in this regard in [60] and [82]: in the first one, the training duration was heuristically set on the basis of the fundamental vibration period of the structure; in the second one, a self-setting strategy was proposed, based on the so-called SVD update [83], to allow reducing the computational costs of training to a minimum. In what follows, results are presented as obtained with the former approach.

4.2. Dual estimation and online updating of the ROM

Moving now to the application of the proposed identification procedure, results are reported next in the case of all the floor lateral displacements gathered in the observation vector $\boldsymbol{y}_k$. It is therefore assumed that the system can be fully observed as far as story lateral displacements are concerned; since the full-order model of the structure gathers not only displacements but also velocities and accelerations for tracking purposes in a stochastic environment, the system is accordingly only partially observed. An optimization procedure to deploy a minimal amount of sensors on the structure is beyond the scope of the present study, and will be addressed in future contributions.

According to what reported, in the analyses it results to be $m = n = N_p = 8$, and the dimension $3l + N_p$ of the joint state vector respectively amounts to 11 if $l = 1$ and to 14 if $l = 2$; cases featuring larger l values have not been considered due to the limited number of storys and to the high energetic accuracy p of the ROMs with $l = 1{,}2$. As far as filtering is concerned, the algorithmic covariance matrices have been set as follows, $\boldsymbol{I}$ being an identity matrix of appropriate dimension: $\boldsymbol{\mathcal{P}}_0 = 10^{-10}\boldsymbol{I}$; $\boldsymbol{\Pi}_0 = 10^{-12}\boldsymbol{I}$; $\boldsymbol{V}^{\varphi} = 10^{-10}\boldsymbol{I}$; $\boldsymbol{V}^{y} = 10^{-5}\boldsymbol{I}$; $\boldsymbol{V}^{\chi}$ diagonal with entries on the order of $10^{-6} - 10^{-8}$ for the structural state $\boldsymbol{\chi}_k$, and $10^{8} - 10^{-10}$ (KN/m)^2 for the stiffness coefficients. The aforementioned noise parameters are called the tuning knobs of the Kalman filter, and most often are adjusted via a trial and error procedure in an offline stage prior to the application of the filter itself [84]. These parameters should be as large as possible to allow the filter to react in real-time (or close to real-time) to the changing environment, but cannot be increased beyond critical thresholds to avoid filter instabilities, and so divergence of the estimates. Recently, handful approaches have been proposed in the literature for the optimal and autonomous tuning of the parameters of recursive Bayesian filters, see [85-89].

The damage event foreseen in Section 4.1 and of an assigned intensity $d = 0.5$, is now assumed to instantaneously occur at $t = 20$ s. Figures 5 and 6 provide for $l = 1$ and $l = 2$ the final estimation of the retained POM(s) at $t = 200$ s, and their evolution along the SHM phase; for comparison purposes, also the initial undamaged solutions at t_0 are reported. It is shown that, in both cases, POM #1 is modified after damage inception; then, convergence to a steady state solution is soon attained. The estimated shape of POM #2 is instead somehow different from the actual one reported in Figure 4; also its time evolution does not provide any evidence of a clear switch to a damage-affected solution. As discussed in Section 3, the POMs here provided for the damaged case have not been obtained by re-training the ROM; instead, they have been continuously updated by the Kalman filter to better match

the measured structural response. Hence, they are provided by the online procedure and do not require additional offline (re-training or post-processing) stages to be completed as soon as a damage evolution is sensed; right after damage inception, some discrepancies with respect to those obtained by re-training the ROM are therefore expected.

In Figure 7, the singular values relevant to the undamaged and damaged states are plotted. This graph is provided to compare the features of the two states, but it must be noted that the values related to the damaged case are never computed in the proposed approach, since the ROM is never re-trained to avoid a loss of computational efficiency. Although the hierarchy of singular values relevant to the virgin state is somehow broken by the considered damage, as evidenced e.g. by the couples of values getting closer in the damaged state, the ROMs built with $l = 1$ and $l = 2$ provide a reasonably high accuracy, always featuring $p > 99$ % as reported in Table 3. So, even if POVs and also natural frequencies are affected by damage, the accuracy of the ROMs does not get reduced significantly by it, thanks to the beneficial effect of Kalman filtering. Such accuracy could be further increased by procedures like that proposed in [62], and based on Ritz vectors possibly featuring appropriate discontinuities at the damage location(s). The relevant topic of ROM enhancement is not addressed in this work, due to the following reasons: as reported, the ROMs given by $l = 1,2$ are already accurate enough to represent the full displacement field, as testified by the relevant p values; Ritz vectors featuring appropriate discontinuities would require the a-priori knowledge of damage location or, conversely, the handling of a set of vectors, each one with a discontinuity at a single inter-story level, with an increase of the overall computational burden. In place of additional modes or pre-defined vectors, the Kalman filter is exploited to progressively increase the accuracy of the ROMs when damage inception/growth gives rise to a drift of the measured structural response away from the expected undamaged one.

The relatively lower contribution of POM #2 to the whole structural response, as shown by Figure 7, is supposed to detrimentally affect the solution in terms of estimated components of the reduced-order stiffness matrix $\boldsymbol{\mathcal{K}}$. Figures 8 and 9 provide charts of the time evolution of such stiffness components, once again for $l = 1$ and $l = 2$ respectively. Although the displayed convergence rate is not high, if $l = 1$ the information content brought by observations allows attaining an almost invariant and unbiased solution within around 50 s. The reduced-order model obtained with $l = 2$ is supposed to feature a higher accuracy concerning the dynamic behavior of the structure and the effects of damage. Accordingly, the convergence rate shown by the $\boldsymbol{\mathcal{K}}$ terms is higher if compared to the case $l = 1$, and a

quasi-stationary solution for the damaged state is attained after around 20 s. But, somehow surprisingly in view of the mentioned higher content of information about the structural properties, the damaged $\boldsymbol{\mathcal{K}}$ terms converge towards a biased solution, which cannot be improved even if observations are continuously handled by the filters. The convergence rates shown in the figures can be somehow improved by increasing the values of the algorithmic filter parameters given above and related to model uncertainties, but at the risk of estimation instability. As already mentioned, the adopted setting implies a trade-off between convergence rate (and so readiness of the identification procedure to soon track damage evolution) and algorithmic stability (to avoid diverging estimates).

To assess the issue of the biased estimates, it is worth noting again that stability and convergence of the Kalman filtering procedure can be difficult to assure in the presence of damage. The stochastic analyses described in [90] and [78] have to account for the uncertainty levels in the state-space formulation, ultimately linked to the process and measurement noises; for the present approach, the additional mutual effects of the two filtering processes running simultaneously and of the reduced-order modeling should be accounted for too. What can be seen in Figure 9 is that the addition of POM #2 to the model, leads to a bias in the estimate of $\mathcal{K}_{11}$. To understand the physical reasons of this outcome, the sensitivity of $\mathcal{K}_{11}$, $\mathcal{K}_{12}$ and $\mathcal{K}_{22}$ to a damage of varying intensity d, located at each inter-story or floor level, is reported in Figure 10. It emerges that $\mathcal{K}_{11}$ smoothly depends on both d and floor index; hence, the identifiability of damage based on the capability of the procedure to discern the effects of damage, looks good. $\mathcal{K}_{12}$ instead does not vary monotonically with the floor index; this is clearly visible for the maximum damage value $d = 0.5$ reported in the graph, but it holds true also for smaller damage values. Such non-monotonic dependence on the floor index looks even enhanced for $\mathcal{K}_{22}$; for this stiffness component, it is further shown that the dependence on d is rather weak if damage is located around the fourth floor.

To show the effects of the mentioned low, or even null sensitivity to damage of $\boldsymbol{\mathcal{K}}$ components, results are depicted in Figure 11 in terms of the lateral displacement at the fifth floor. The time evolution of it is given, as provided by the trained ROM and by additional models whose components of the stiffness matrix have been in turn artificially modified by $\pm 10\%$; for comparison purposes and to also assess the accuracy of the POD-based model, the same time history is also shown as furnished by the full-order model. Graphs show that the variations of $\mathcal{K}_{11}$ effectively modify the time history, whereas variations of $\mathcal{K}_{12}$ and $\mathcal{K}_{22}$ do not: in these last two cases, results all look almost perfectly superposed to each other. This outcome has been selected to show a kind of pathological feature of the ROM at the

considered floor; since all the story displacements are collected in the measurement vector $\boldsymbol{y}_k$, the null sensitivity at this floor is partially compensated for by the algorithm through the exploitation of measurements collected elsewhere. Such strategy is in line with the mentioned requirement of redundancy in the observables.

To assess the capability of the approach to track the whole structural dynamics, granted that only measurements of the story displacements are collected in $\boldsymbol{y}_k$, results are reported in Figure 12 in terms of estimated displacement, velocity and acceleration at the fifth floor, for $l = 1$ and $l = 2$; the target time evolutions are also given for comparison. Very similar results can be reported for all the other storys. The figure provides close-ups at three different stages of the analysis: at the beginning of the excitation, where a steady-state solution is not attained yet, and ROMs might fail to catch the effects of higher-order vibration modes; around the inception of the damage event, to show that within a short time interval after $t = 20$ s the estimated state converges towards the target; close to the end of the analysis, to also show that in the long-time range the estimates are not spoiled by error accumulation, and so do not lead to dangerous artificial drifts from the target structural response that can be interpreted by the SHM procedure as a growing damage. As for this task, graphs clearly show that, by increasing the order l of the model, the accuracy of the estimates gets increased too.

In Figure 13 phase-space plots relevant to the same fifth floor are reported, to further assess the performance of the proposed approach in tracking the structural state. As already shown by Figure 12, the accuracy in terms of tracked displacement (the observed state component) is the highest. The plot provided by the proposed filtering procedure does not perfectly match the target solution, especially in the case $l = 1$; anyhow, as in any joint system identification procedure, the overall accuracy of state tracking gets enhanced as time grows and additional observations are handled. This outcome, which is partially hidden in Figure 13 by the discrepancy between target and identified solutions at the beginning of the identification phase, has been clearly shown by the time histories of Figure 12.

As discussed in Section 4.1, a change in the value of the stiffness parameters or in the slope of POMs of the ROM is a damage signal. However, in order to quantify the severity of the damage one needs to establish a relationship among a set of damage indices, the POMs and the stiffness parameters in the damaged state(s). A common method for damage identification by exploiting the tracked changes in the vibration characteristics of the structure, is based on artificial neural networks, see e.g. [91,92].

Finally, concerning the speed-up provided by the reduced-order modeling, results are compared in Table 3 as obtained through both floating-point operation and CPU time metrics. Data have been obtained by running the procedure implemented in MATLAB (release 2010a) on a personal computer featuring an Intel Core (TM) i7-2630 QM @ 2.00 GHz processor, with 8.00 GB of RAM and Windows 7 64-bit as OS. As already highlighted in [76], Table 3 shows that the speed-up computed through the algorithmic complexity represents an upper bound on the real one; although an implementational optimization of the code can be foreseen to provide better outcomes, a noteworthy computational gain is reported.

6. Conclusion

In this paper, an approach for the concurrent dual estimation and reduced-order modelling of a damaging structure has been proposed. As for the reduced-order modelling task, proper orthogonal decomposition has been adopted to define the subspace that optimally captures the dynamics of the system. As for the dual estimation task, an extended Kalman filter has been instead adopted. When the identification of a ROM is studied, a reconstruction of full state of the system is required to compare the latest observations with the relevant filter prediction; this looks possible only if the subspace is known.

In the case of a damaging structure, the proposed approach can automatically update the ROM through an additional Kalman filter. The relevant online tuning of the ROM, without any need of time consuming re-training stages, has been shown to allow the detection of damage in the structure, in terms of both location and (potentially) intensity.

In future works, the proposed approach will be extended to deal with more complex, real-life applications. An explicit identification of the damage state will be allowed for by appropriately modifying the augmented state vector handled by the intricate Bayesian procedure: identifiability of damage, linked to the optimal deployment of a sensor network, and reduced-order modeling featuring minimal dimension, will be fully addressed.

Acknowledgments

Financial support by Fondazione Cariplo through project Safer Helmets is gratefully acknowledged.

References

1. Glaser, S.D., Li, H., Wang, M.L., Ou, J., Lynch, J.: Sensor technology innovation for the advancement of structural health monitoring: a strategic program of US-China research for the next decade. Smart Structures and Systems **3**(2), 221-244 (2007). doi:http://dx.doi.org/10.12989/sss.2007.3.2.221
2. Stallings, J.M., Tedesco, J.W., El-Mihilmy, M., McCauley, M.: Field performance of FRP bridge repairs. Journal of Bridge Engineering **5**, 107–113 (2000).
3. Aktan, A., Catbas, F., Grimmelsman, K., Tsikos, C.: Issues in Infrastructure Health Monitoring for Management. Journal of Engineering Mechanics **126**(7), 711-724 (2000). doi:10.1061/(ASCE)0733-9399(2000)126:7(711)
4. Ko, J.M., Ni, Y.Q.: Technology developments in structural health monitoring of large-scale bridges. Engineering Structures **27**(12), 1715-1725 (2005). doi:http://dx.doi.org/10.1016/j.engstruct.2005.02.021
5. Glaser, S.D., Tolman, A.: Sense of Sensing: From Data to Informed Decisions for the Built Environment. Journal of Infrastructure Systems ACSE **14**, 4-14 (2008).
6. Yeum, C.M., Dyke, S.J.: Vision-Based Automated Crack Detection for Bridge Inspection. Computer-Aided Civil and Infrastructure Engineering **30**(10), 759-770 (2015). doi:10.1111/mice.12141
7. Memarzadeh, M., Pozzi, M.: Integrated Inspection Scheduling and Maintenance Planning for Infrastructure Systems. Computer-Aided Civil and Infrastructure Engineering, n/a-n/a (2015). doi:10.1111/mice.12178
8. Cho, S., Spencer, B.F.: Sensor Attitude Correction of Wireless Sensor Network for Acceleration-Based Monitoring of Civil Structures. Computer-Aided Civil and Infrastructure Engineering **30**(11), 859-871 (2015). doi:10.1111/mice.12147
9. Mariani, S., Corigliano, A., Caimmi, F., Bruggi, M., Bendiscioli, P., De Fazio, M.: MEMS-based surface mounted health monitoring system for composite laminates. Microelectronics Journal **44**(7), 598-605 (2013). doi:http://dx.doi.org/10.1016/j.mejo.2013.03.003
10. Mariani, S., Bruggi, M., Caimmi, F., Bendiscioli, P., De Fazio, M.: Sensor deployment over damage-containing plates: a topology optimization approach. Journal of Intelligent Material Systems and Structures **24**, 1105–1122 (2013).
11. Chan, T.H.T., Yu, L., Tam, H.Y., Ni, Y.Q., Liu, S.Y., Chung, W.H., Cheng, L.K.: Fiber Bragg grating sensors for structural health monitoring of Tsing Ma bridge: Background and experimental observation. Engineering Structures **28**(5), 648-659 (2006). doi:10.1016/j.engstruct.2005.09.018
12. Helmi, K., Taylor, T., Zarafshan, A., Ansari, F.: Reference free method for real time monitoring of bridge deflections. Engineering Structures **103**, 116-124 (2015). doi:10.1016/j.engstruct.2015.09.002
13. Hampshire, T.A., Adeli, H.: Monitoring the behavior of steel structures using distributed optical fiber sensors. Journal of Constructional Steel Research **53**(3), 267-281 (2000).
14. Gentile, C., Cabboi, A.: Vibration-based structural health monitoring of stay cables by microwave remote sensing. Smart Structures and Systems **16**(2), 263-280 (2015). doi:http://dx.doi.org/10.12989/sss.2015.16.2.263
15. Farrar, C.R., Darling, T.W., Migliori, A., Baker, W.E.: Microwave interferometers for non-contact vibration measurements on large structures. Mechanical Systems and Signal Processing **13**(2), 241-253 (1999). doi:10.1006/mssp.1998.1216

16. Laefer, D.F., Truong-Hong, L., Carr, H., Singh, M.: Crack detection limits in unit based masonry with terrestrial laser scanning. NDT and E International **62**, 66-76 (2014). doi:10.1016/j.ndteint.2013.11.001
17. Breuer, P., Chmielewski, T., Górski, P., Konopka, E.: Application of GPS technology to measurements of displacements of high-rise structures due to weak winds. Journal of Wind Engineering and Industrial Aerodynamics **90**(3), 223-230 (2002). doi:10.1016/S0167-6105(01)00221-5
18. Górski, P.: Investigation of dynamic characteristics of tall industrial chimney based on GPS measurements using Random Decrement Method. Engineering Structures **83**, 30-49 (2015). doi:http://dx.doi.org/10.1016/j.engstruct.2014.11.006
19. Park, S.W., Park, H.S., Kim, J.H., Adeli, H.: 3D displacement measurement model for health monitoring of structures using a motion capture system. Measurement **59**, 352-362 (2015). doi:http://dx.doi.org/10.1016/j.measurement.2014.09.063
20. Lee, J.J., Shinozuka, M.: Real-time displacement measurement of a flexible bridge using digital image processing techniques. Experimental Mechanics **46**(1), 105-114 (2006). doi:10.1007/s11340-006-6124-2
21. Hwa Kim, B.: Extracting modal parameters of a cable on shaky motion pictures. Mechanical Systems and Signal Processing **49**(1-2), 3-12 (2014). doi:10.1016/j.ymssp.2014.02.002
22. Qarib, H., Adeli, H.: Recent advances in health monitoring of civil structures. Scientia Iranica **21**(6), 1733-1742 (2014).
23. Bursi, O.S., Kumar, A., Abbiati, G., Ceravolo, R.: Identification, model updating, and validation of a steel twin deck curved cable-stayed footbridge. Computer-Aided Civil and Infrastructure Engineering **29**(9), 703-722 (2014). doi:10.1111/mice.12076
24. Fuggini, C., Chatzi, E., Zangani, D.: Combining Genetic Algorithms with a Meso-Scale Approach for System Identification of a Smart Polymeric Textile. Computer-Aided Civil and Infrastructure Engineering **28**(3), 227-245 (2013). doi:10.1111/j.1467-8667.2012.00789.x
25. Moaveni, B., Conte, J.P., Hemez, F.M.: Uncertainty and Sensitivity Analysis of Damage Identification Results Obtained Using Finite Element Model Updating. Computer-Aided Civil and Infrastructure Engineering **24**(5), 320-334 (2009). doi:10.1111/j.1467-8667.2008.00589.x
26. Moaveni, B., Behmanesh, I.: Effects of changing ambient temperature on finite element model updating of the Dowling Hall Footbridge. Engineering Structures **43**, 58-68 (2012).
27. Farrar, C.R., Doebling, S.W., Nix, D.A.: Vibration–based structural damage identification. Philosophical Transactions of the Royal Society of London A: Mathematical, Physical and Engineering Sciences **359**(1778), 131-149 (2001).
28. Haritos, N., Owen, J.S.: The Use of Vibration Data for Damage Detection in Bridges: A Comparison of System Identification and Pattern Recognition Approaches. Structural Health Monitoring **3**(2), 141-163 (2004). doi:10.1177/1475921704042698
29. Farrar, C.R., Worden, K.: Structural Health Monitoring: A Machine Learning Perspective. Structural Health Monitoring: A Machine Learning Perspective. Wiley Publishing, (2012)
30. Amezquita-Sanchez, J.P., Adeli, H.: Signal Processing Techniques for Vibration-Based Health Monitoring of Smart Structures. Archives of Computational Methods in Engineering **23**(1), 1-15 (2016). doi:10.1007/s11831-014-9135-7
31. Dervilis, N., Worden, K., Cross, E.: On robust regression analysis as a means of exploring environmental and operational conditions for SHM data. Journal of Sound and Vibration **347**, 279-296 (2015).

32. Spiridonakos, M.D., Chatzi, E.N., Sudret, B.: Polynomial Chaos Expansion Models for the Monitoring of Structures under Operational Variability. ASCE-ASME Journal of Risk and Uncertainty in Engineering Systems, Part A: Civil Engineering, B4016003 (2016).
33. Reynders, E., Wursten, G., De Roeck, G.: Output-only structural health monitoring in changing environmental conditions by means of nonlinear system identification. Structural Health Monitoring **13**(1), 82-93 (2014).
34. Yang, J., Lin, S.: Identification of Parametric Variations of Structures Based on Least Squares Estimation and Adaptive Tracking Technique. Journal of Engineering Mechanics **131**(3), 290-298 (2005). doi:doi:10.1061/(ASCE)0733-9399(2005)131:3(290)
35. Van Overschee, P., De Moor, B.: Subspace Identification for Linear Systems: Theory — Implementation — Applications. Springer US, (1996)
36. Van Overschee, P., De Moor, B.: N4SID: Subspace algorithms for the identification of combined deterministic-stochastic systems. Automatica **30**(1), 75-93 (1994). doi:http://dx.doi.org/10.1016/0005-1098(94)90230-5
37. Chin-Hsiung, L., Jian-Huang, W., Yi-Cheng, L., Pei-Yang, L., Shieh-Kung, H.: Structural damage diagnosis based on on-line recursive stochastic subspace identification. Smart Materials and Structures **20**(5), 055004 (2011).
38. Chatzis, M., Chatzi, E., Smyth, A.W.: An experimental validation of time domain system identification methods with fusion of heterogeneous data. Earthquake Engineering and Structural Dynamics **44**(4), 523-547 (2015). doi:10.1002/eqe.2528
39. Moaveni, B., He, X., Conte, J., Restrepo, J., Panagiotou, M.: System Identification Study of a 7-Story Full-Scale Building Slice Tested on the UCSD-NEES Shake Table. Journal of Structural Engineering **137**(6), 705-717 (2010). doi:10.1061/(ASCE)ST.1943-541X.0000300
40. Kalman, R.E.: A new approach to linear filtering and prediction problems. Journal of basic Engineering **82**(1), 35-45 (1960).
41. Julier, S.J., Uhlmann, J.K.: A new extension of the Kalman filter to nonlinear systems. In: Int. symp. aerospace/defense sensing, simul. and controls 1997, vol. 26, p. 32. Orlando, FL
42. Gordon, N.J., Salmond, D.J., Smith, A.F.M.: Novel approach to nonlinear/non-Gaussian Bayesian state estimation. Radar and Signal Processing, IEE Proceedings F **140**(2), 107-113 (1993).
43. Chatzi, E.N., Smyth, A.W.: Particle filter scheme with mutation for the estimation of time-invariant parameters in structural health monitoring applications. Structural Control and Health Monitoring **20**(7), 1081-1095 (2013).
44. Li, B.: Multiple-model Rao-Blackwellized particle CPHD filter for multitarget tracking. Nonlinear Dynamics **79**(3), 2133-2143 (2014). doi:10.1007/s11071-014-1799-x
45. Eftekhar Azam, S., Mariani, S.: Dual estimation of partially observed nonlinear structural systems: A particle filter approach. Mechanics Research Communications **46**, 54-61 (2012).
46. Chatzi, E.N., Smyth, A.W., Masri, S.F.: Experimental application of on-line parametric identification for nonlinear hysteretic systems with model uncertainty. Structural Safety **32**(5), 326-337 (2010).
47. Eftekhar Azam, S.: Online damage detection in structural systems. SpringerBriefs in Applied Sciences and Technology. Springer, (2014)
48. Kerschen, G., Golinval, J.-c., Vakakis, A.F., Bergman, L.A.: The method of proper orthogonal decomposition for dynamical characterization and order reduction of mechanical systems: an overview. Nonlinear dynamics **41**(1-3), 147-169 (2005).

49. Lu, K., Yu, H., Chen, Y., Cao, Q., Hou, L.: A modified nonlinear POD method for order reduction based on transient time series. Nonlinear Dynamics **79**(2), 1195-1206 (2014). doi:10.1007/s11071-014-1736-z
50. Lu, K., Jin, Y., Chen, Y., Cao, Q., Zhang, Z.: Stability analysis of reduced rotor pedestal looseness fault model. Nonlinear Dynamics **82**(4), 1611-1622 (2015). doi:10.1007/s11071-015-2264-1
51. Zhao, X., Shang, P.: Principal component analysis for non-stationary time series based on detrended cross-correlation analysis. Nonlinear Dynamics **84**(2), 1033-1044 (2015). doi:10.1007/s11071-015-2547-6
52. Liang, Y.C., Lin, W.Z., Lee, H.P., Lim, S.P., Lee, K.H., Sun, H.: Proper Orthogonal Decomposition And Its Applications – Part Ii: Model Reduction For Mems Dynamical Analysis. Journal of Sound and Vibration **256**(3), 515-532 (2002). doi:http://dx.doi.org/10.1006/jsvi.2002.5007
53. Ruotolo, R., Surace, C.: Using svd to detect damage in structures with different operational conditions. Journal of Sound and Vibration **226**(3), 425-439 (1999). doi:http://dx.doi.org/10.1006/jsvi.1999.2305
54. Vanlanduit, S., Parloo, E., Cauberghe, B., Guillaume, P., Verboven, P.: A robust singular value decomposition for damage detection under changing operating conditions and structural uncertainties. Journal of Sound and Vibration **284**(3–5), 1033-1050 (2005). doi:http://dx.doi.org/10.1016/j.jsv.2004.07.016
55. Galvanetto, U., Violaris, G.: Numerical investigation of a new damage detection method based on proper orthogonal decomposition. Mechanical Systems and Signal Processing **21**(3), 1346-1361 (2007). doi:http://dx.doi.org/10.1016/j.ymssp.2005.12.007
56. Shane, C., Jha, R.: Proper orthogonal decomposition based algorithm for detecting damage location and severity in composite beams. Mechanical Systems and Signal Processing **25**(3), 1062-1072 (2011). doi:http://dx.doi.org/10.1016/j.ymssp.2010.08.015
57. Mariani, S., Ghisi, A.: Unscented Kalman filtering for nonlinear structural dynamics. Nonlinear Dynamics **49**(1-2), 131-150 (2007).
58. Hughes, T.J.R.: The Finite Element Method. Linear Static and Dynamic Finite Element Analysis Dover, New York (2000)
59. Corigliano, A., Mariani, S.: Parameter identification in explicit structural dynamics: performance of the extended Kalman filter. Computer Methods in Applied Mechanics and Engineering **193**, 3807-3830 (2004).
60. Eftekhar Azam, S., Mariani, S.: Investigation of computational and accuracy issues in POD-based reduced order modeling of dynamic structural systems. Engineering Structures **54**, 150-167 (2013).
61. Butcher, E.A., Al-Shudeifat, M.A.: An efficient mode-based alternative to principal orthogonal modes in the order reduction of structural dynamic systems with grounded nonlinearities. Mechanical Systems and Signal Processing **25**(5), 1527-1549 (2011).
62. Al-Shudeifat, M.A., Butcher, E.A.: Order reduction of forced nonlinear systems using updated LELSM modes with new Ritz vectors. Nonlinear Dynamics **62**(4), 821-840 (2010).
63. Kappagantu, R., Feeny, B.: An" optimal" modal reduction of a system with frictional excitation. Journal of Sound and Vibration **224**(5), 863-877 (1999).
64. Al-Shudeifat, M.A., Butcher, E.A.: On the dynamics of a beam with switching crack and damaged boundaries. Journal of Vibration and Control, 1077546311428640 (2011).
65. Feeny, B., Kappagantu, R.: On the physical interpretation of proper orthogonal modes in vibrations. Journal of sound and vibration **211**(4), 607-616 (1998).

66. Han, C.S., Feeny, B.: Enhanced proper orthogonal decomposition for the modal analysis of homogeneous structures. Journal of Vibration and Control **8**(1), 19-40 (2002).
67. Feeny, B.: On proper orthogonal co-ordinates as indicators of modal activity. Journal of Sound and Vibration **255**(5), 805-817 (2002).
68. Corigliano, A., Dossi, M., Mariani, S.: Model order reduction and domain decomposition strategies for the solution of the dynamic elastic-plastic structural problem. Computer Methods in Applied Mechanics and Engineering **290**, 127-155 (2015). doi:10.1016/j.cma.2015.02.021
69. Kerschen, G., Golinval, G.C.: Physical interpretation of the proper orthogonal modes using the singular value decomposition. Journal of Sound and Vibration **249**, 849-865 (2002).
70. Sirovich, L.: Turbulence and the dynamics of coherent structures. I - Coherent structures. II - Symmetries and transformations. III - Dynamics and scaling. Quarterly of Applied Mathematics **45**(1), 573-590 (1987).
71. Liang, Y.C., Lee, H.P., Lim, S.P., Lin, W.Z., Lee, K.H., Wu, C.G.: Proper Orthogonal Decomposition And Its Applications—Part I: Theory. Journal of Sound and Vibration **252**(3), 527-544 (2002). doi:http://dx.doi.org/10.1006/jsvi.2001.4041
72. Bryson, A., Johansen, D.: Linear filtering for time-varying systems using measurements containing colored noise. IEEE Transactions on Automatic Control **10**(1), 4-10 (1965). doi:10.1109/TAC.1965.1098063
73. Geist, M., Pietquin, O.: Kalman filtering & colored noises: the (autoregressive) moving-average case. In: IEEE Workshop on Machine Learning Algorithms, Systems and Applications (MLASA 2011), Honolulu, United States 2011, pp. 1-4
74. Grewal, M.S., Andrews, A.P.: Kalman Filtering: Theory and Practice Using MATLAB, 4th ed. Wiley Publishing, (2011)
75. Wan, E.A., Nelson, A.T.: Dual Extended Kalman Filter Methods. In: Haykin, S. (ed.) Kalman Filtering and Neural Networks. Wiley Publishing, (2001)
76. Capellari, G., Eftekhar Azam, S., Mariani, S.: Damage Detection in Flexible Plates through Reduced-Order Modeling and Hybrid Particle-Kalman Filtering. Sensors **16**(1), 2 (2016). doi:10.3390/s16010002
77. Roffel, A.J., Narasimhan, S.: Extended Kalman filter for modal identification of structures equipped with a pendulum tuned mass damper. Journal of Sound and Vibration **333**(23), 6038-6056 (2014). doi:http://dx.doi.org/10.1016/j.jsv.2014.06.030
78. Reif, K., Gunther, S., Yaz, E., Unbehauen, R.: Stochastic stability of the discrete-time extended Kalman filter. IEEE Transactions on Automatic Control **44**(4), 714-728 (1999). doi:10.1109/9.754809
79. Sharma, G., Agarwala, A., Bhattacharya, B.: A fast parallel Gauss Jordan algorithm for matrix inversion using CUDA. Computers & Structures **128**, 31–37 (2013).
80. De Callafon, R.A., Moaveni, B., Conte, J.P., He, X., Udd, E.: General realization algorithm for modal identification of linear dynamic systems. Journal of Engineering Mechanics **134**(9), 712-722 (2008).
81. Krajcinovic, D.: Damage mechanics. Mechanics of Materials **8**(2-3), 117-197 (1989).
82. Corigliano, A., Dossi, M., Mariani, S.: Domain decomposition and model order reduction methods applied to the simulation of multiphysics problems in MEMS. Computers and Structures **122**, 113-127 (2013).
83. Brand, M.: Fast low-rank modifications of the thin singular value decomposition. Linear Algebra and its Applications **415**, 20-30 (2006).

84. Bittanti, S., Savaresi, S.M.: On the parameterization and design of an extended Kalman filter frequency tracker. IEEE Transactions on Automatic Control **45**(9), 1718-1724 (2000).
85. Kontoroupi, K., Smyth, A.W.: Online noise identification for joint state and parameter estimation of nonlinear systems. ASCE-ASME Journal of Risk and Uncertainty in Engineering Systems **in press**, B4015006 (2015). doi:10.1061/AJRUA6.0000839
86. Yuen, K.-V., Liang, P.F., Kuok, S.C.: Online estimation of noise parameters for Kalman filter. Structural Engineering and Mechanics **47**(3), 361-381 (2013).
87. Yuen, K.-V., Kuok, S.-C.: Online updating and uncertainty quantification using nonstationary output-only measurement. Mechanical Systems and Signal Processing **66–67**, 62-77 (2016). doi:http://dx.doi.org/10.1016/j.ymssp.2015.05.019
88. Lim, J.: Particle filtering for nonlinear dynamic state systems with unknown noise statistics. Nonlinear Dynamics **78**(2), 1369-1388 (2014). doi:10.1007/s11071-014-1523-x
89. Yang, Y., Gao, W.: An optimal adaptive Kalman filter. Journal of Geodesy **80**(4), 177-183 (2006).
90. Boutayeb, M., Rafaralahy, H., Darouach, M.: Convergence analysis of the extended Kalman filter used as an observer for nonlinear deterministic discrete-time systems. IEEE Transactions on Automatic Control **42**(4), 581-586 (1997). doi:10.1109/9.566674
91. Zang, C., Imregun, M.: Structural damage detection using artificial neural networks and measured FRF data reduced via principal component projection. Journal of Sound and Vibration **242**(5), 813-827 (2001).
92. Sahin, M., Shenoi, R.: Quantification and localisation of damage in beam-like structures by using artificial neural networks with experimental validation. Engineering Structures **25**(14), 1785-1802 (2003).

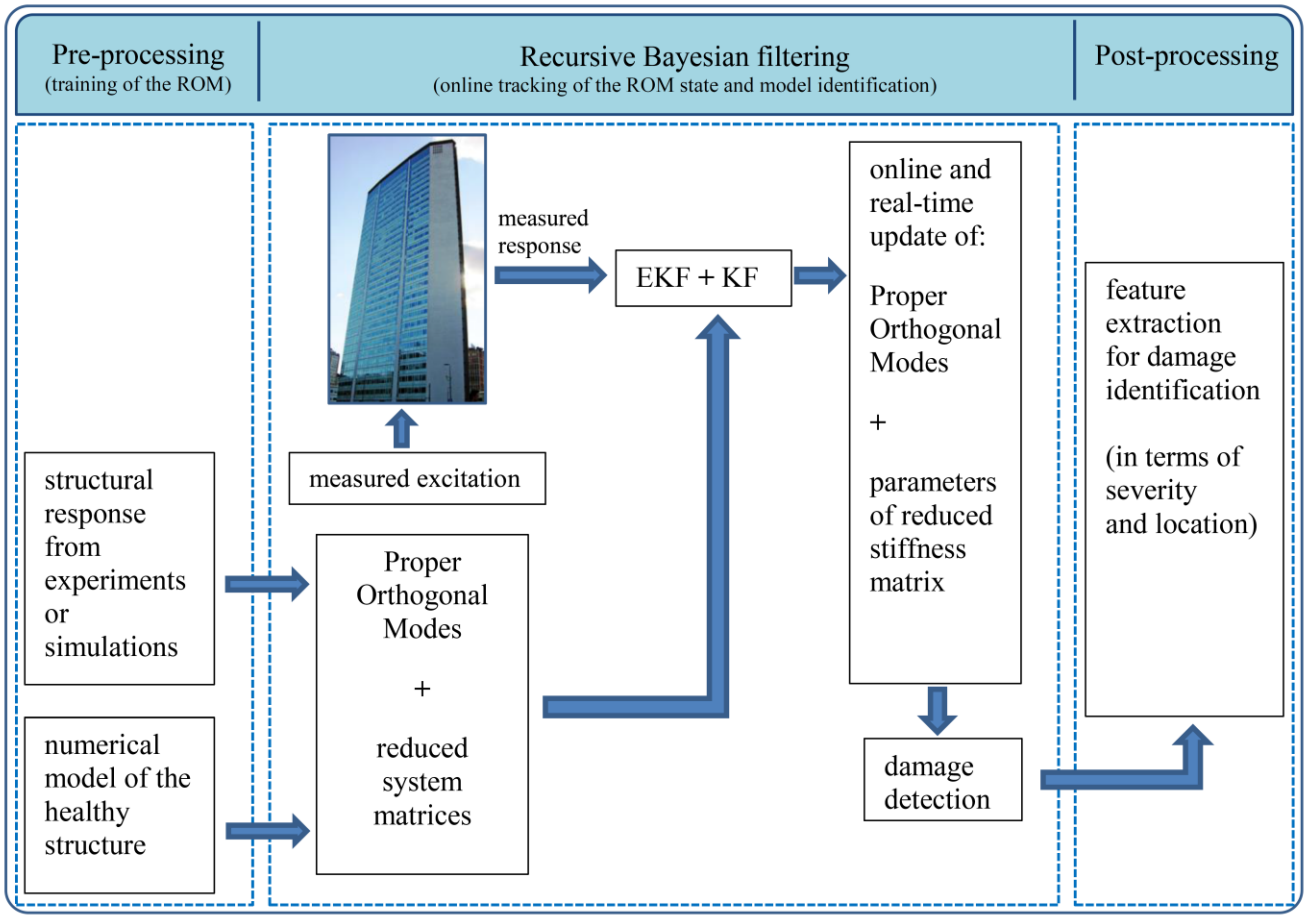

Figure 1. Simplified flowchart of the proposed procedure.

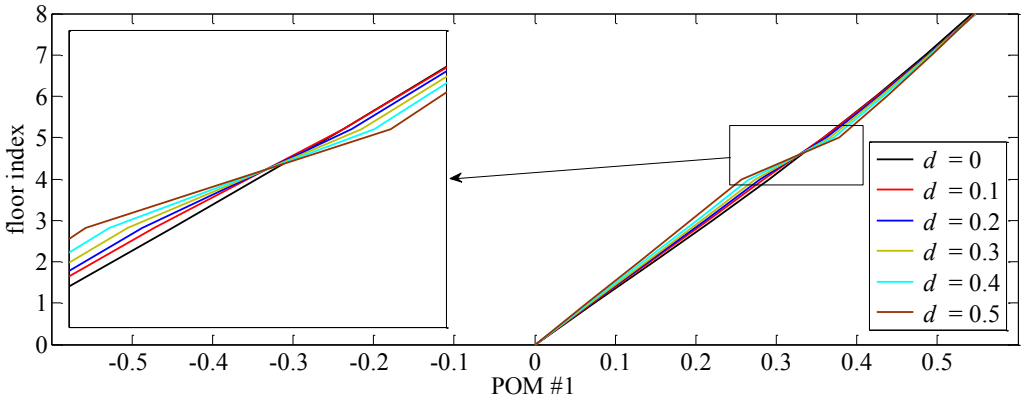

Figure 2. $l = 1$: trained POM for the undamaged structure (black line), and for a damage of varying intensity d located at the inter-story between fourth and fifth floors.

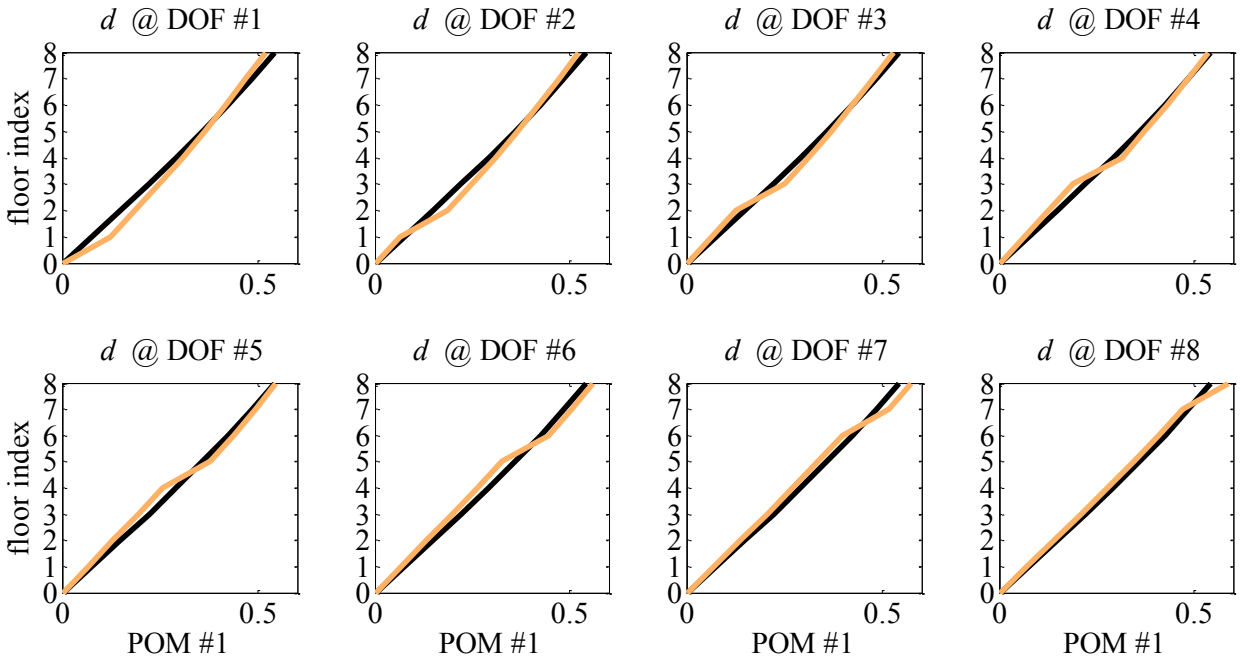

Figure 3. $l = 1$: trained POM for the undamaged structure (black line), and for a damage $d = 0.5$ (orange line) located at a varying inter-story level.

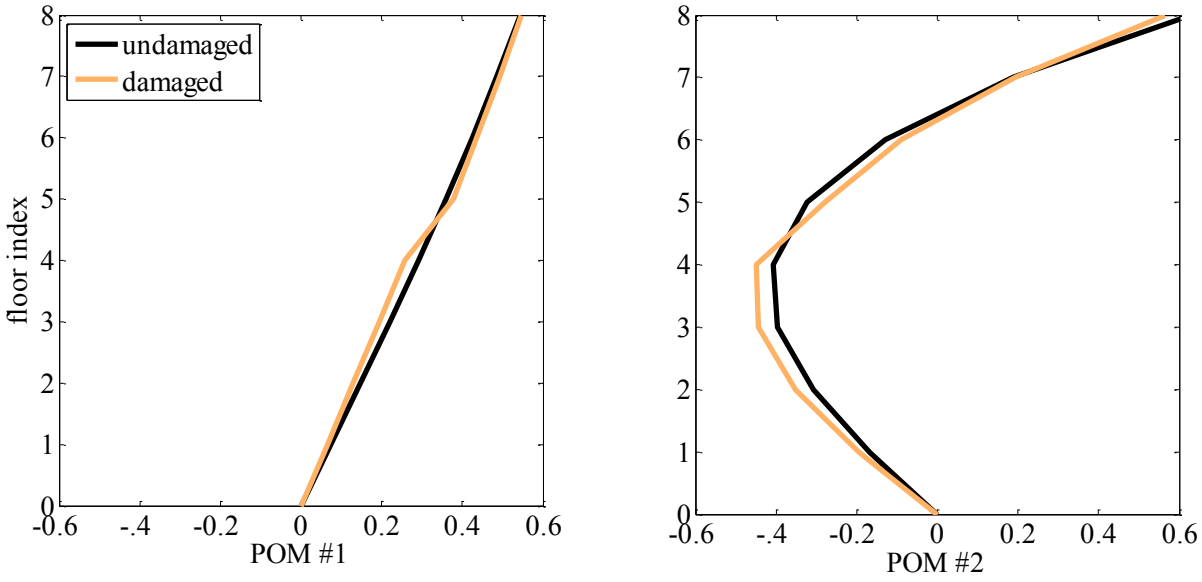

Figure 4. $l = 2$: trained POMs for the undamaged structure (black line), and for a damage $d = 0.5$ (orange line) located at the inter-story between fourth and fifth floors.

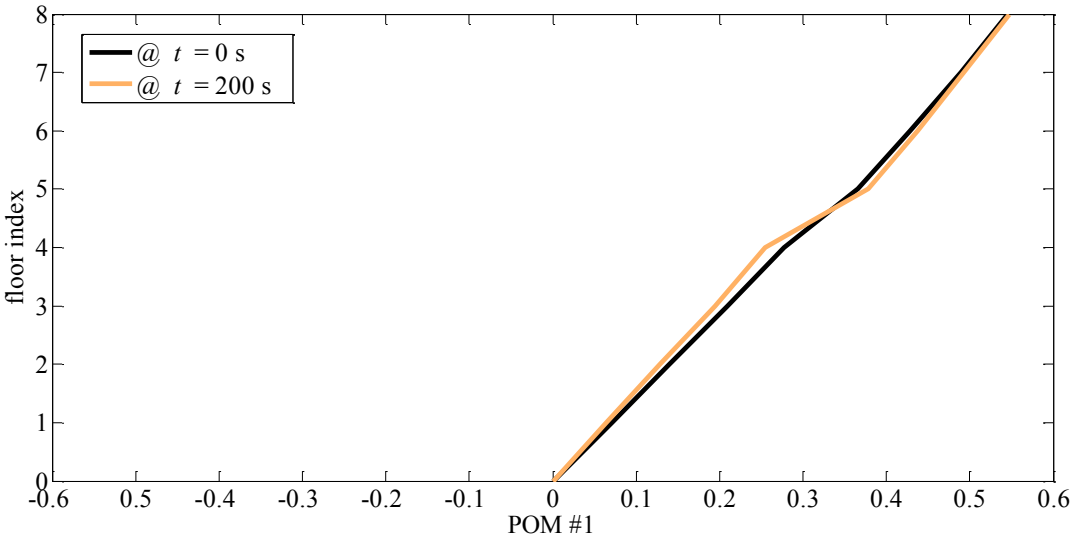

(a)

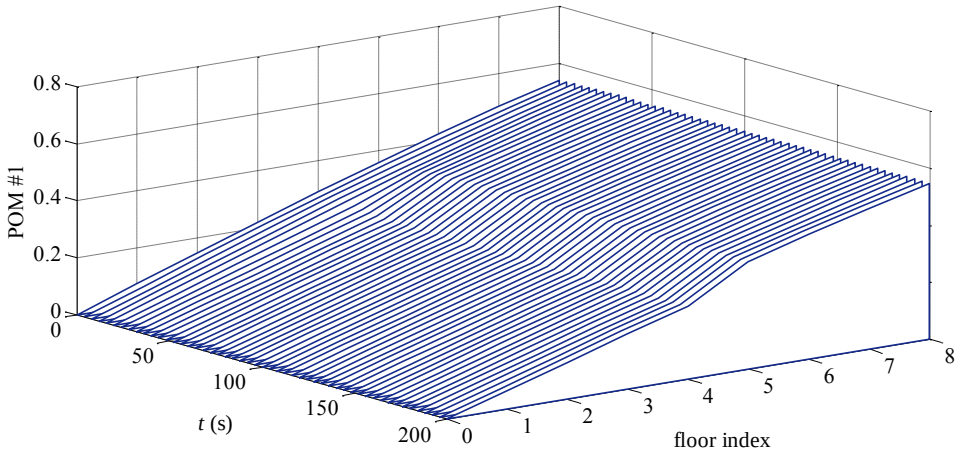

(b)

Figure 5. $l = 1$, damage $d = 0.5$ located at the inter-story between fourth and fifth floors: (a) comparison between the trained POM for the undamaged structure (black line) and the finally indentified POM for the damaged structure (orange line); (b) time evolution of the POM estimate.

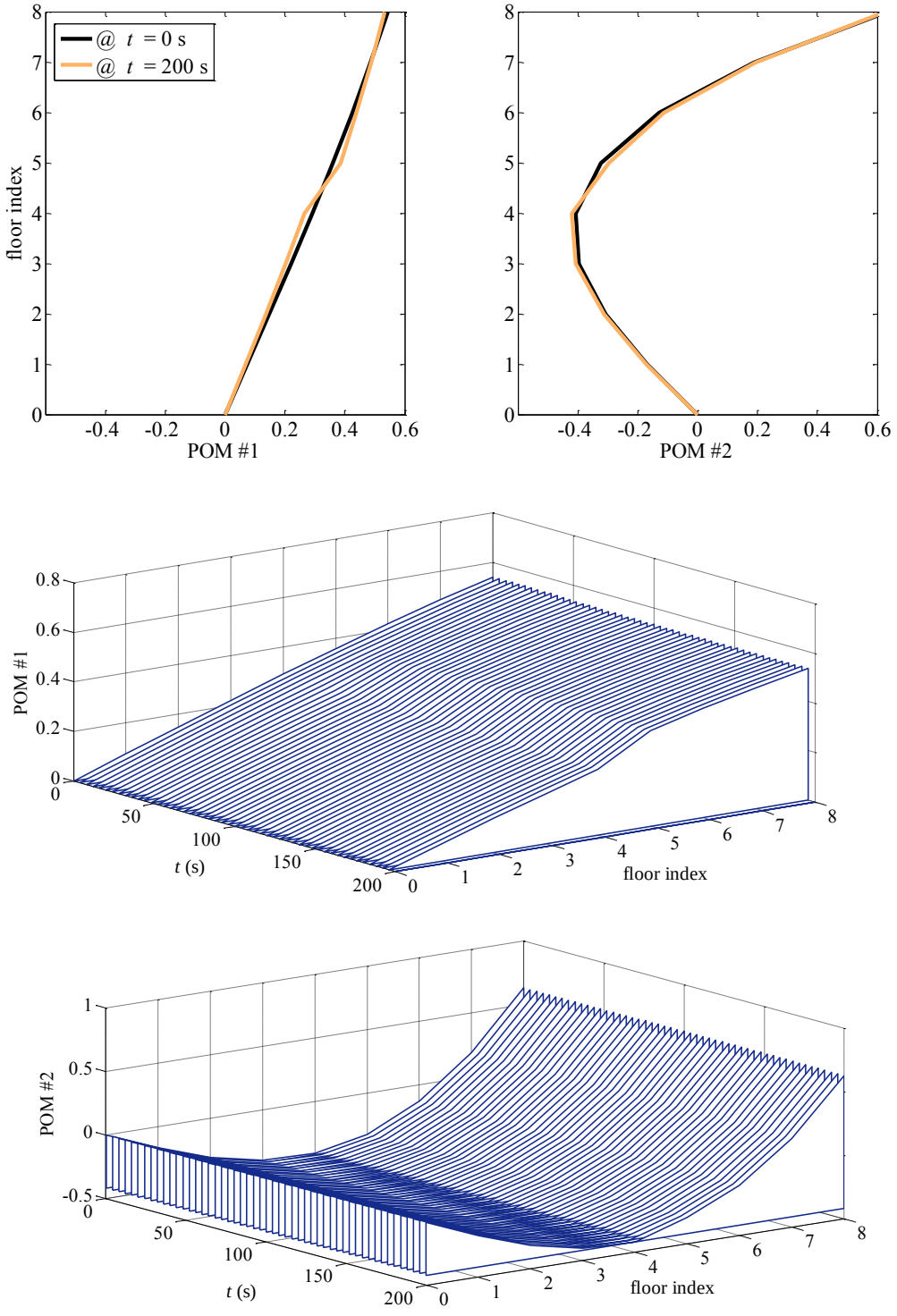

Figure 6. $l = 2$, damage $d = 0.5$ located at the inter-story between fourth and fifth floors: (a) comparison between the trained POMs for the undamaged structure (black lines) and the finally indentified POMs for the damaged structure (orange lines); (b) time evolutions of the POM estimates.

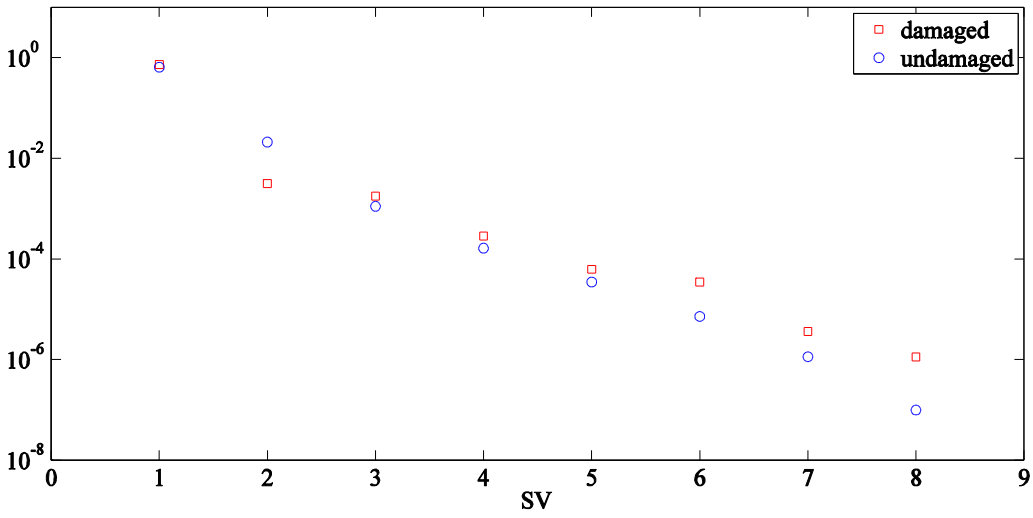

Figure 7. Damage $d = 0.5$ located at the inter-story between fourth and fifth floors: singular values for the undamaged and damaged states.

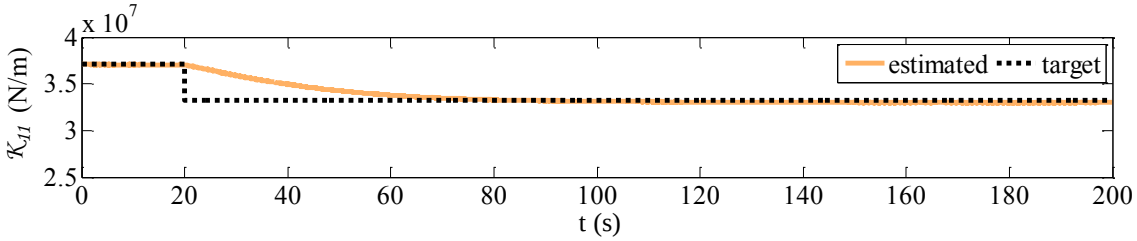

Figure 8. $l = 1$, damage $d = 0.5$ located at the inter-story between fourth and fifth floors: time history of the estimated component $\mathcal{K}_{11}$ of the reduced-order stiffness matrix.

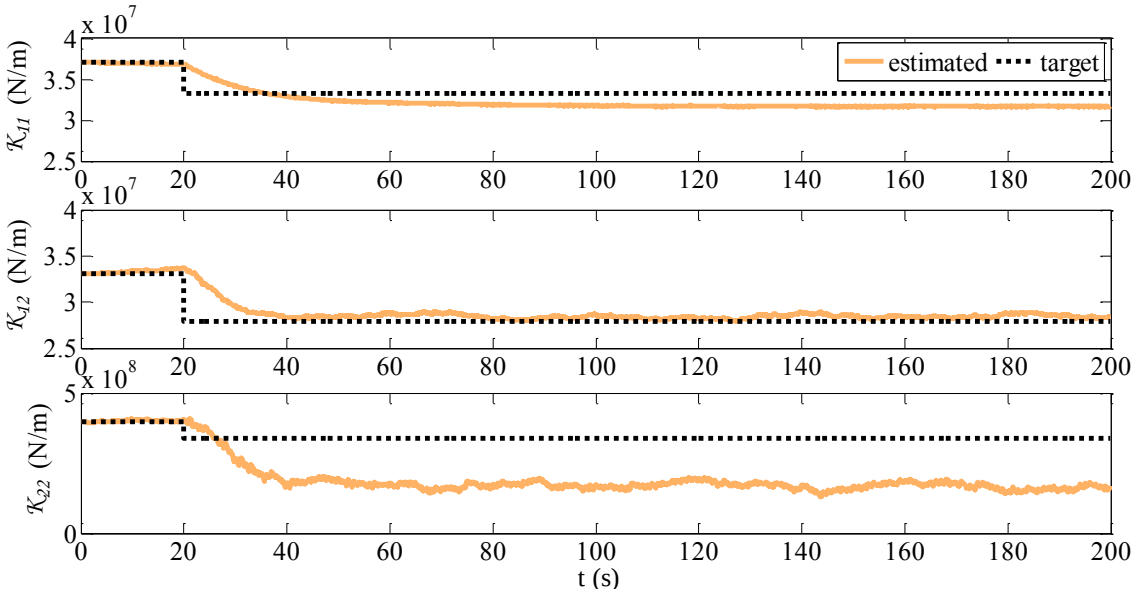

Figure 9. $l = 2$, damage $d = 0.5$ located at the inter-story between fourth and fifth floors: time history of the estimated components $\mathcal{K}_{11}$, $\mathcal{K}_{12}$ and $\mathcal{K}_{22}$ of the reduced-order stiffness matrix.

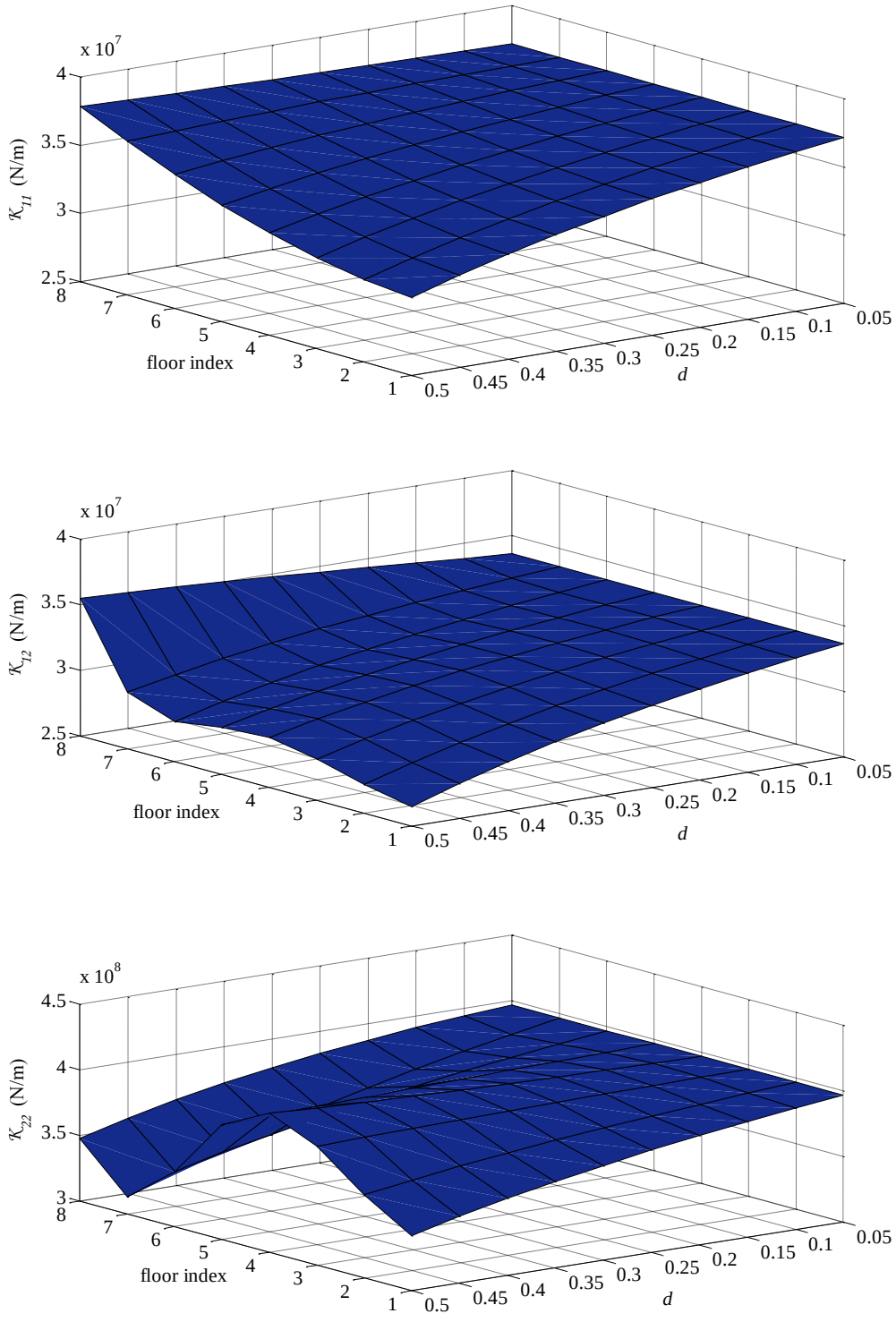

Figure 10. $l = 2$: sensitivity of the components $\mathcal{K}_{11}$, $\mathcal{K}_{12}$ and $\mathcal{K}_{22}$ of the reduced-order stiffness matrix to a damage of varying location and intensity d.

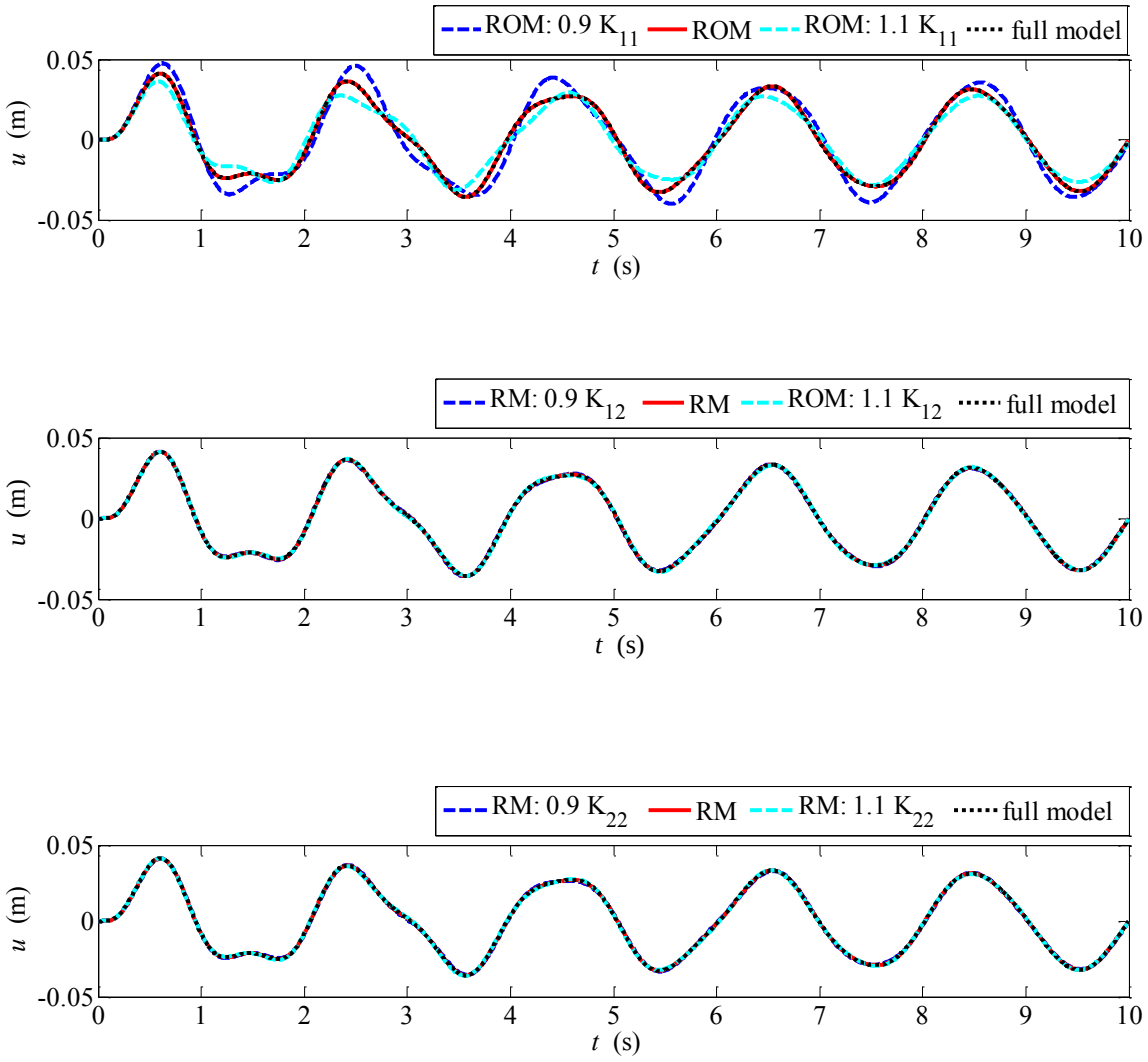

Figure 11. $l = 2$: sensitivity of the time history of displacement at the fifth floor to a damage-induced variation of the components (a) $\mathcal{K}_{11}$, (b) $\mathcal{K}_{12}$ and (c) $\mathcal{K}_{22}$ of the reduced-order stiffness matrix.

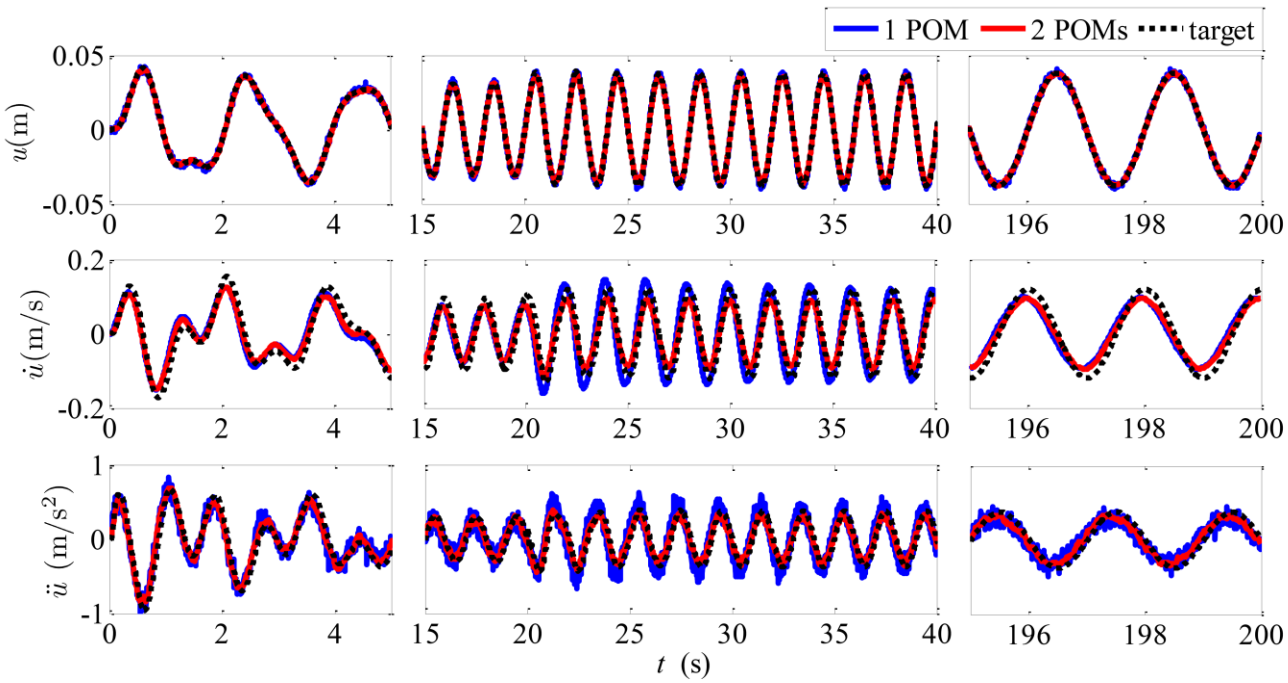

Figure 12. Damage $d = 0.5$ located at the inter-story between fourth and fifth floors: time histories of dispacement, velocity and acceleration at the fifth floor, and comparison among the target solution (black dotted line) and estimated ones at varying order l of the ROM.

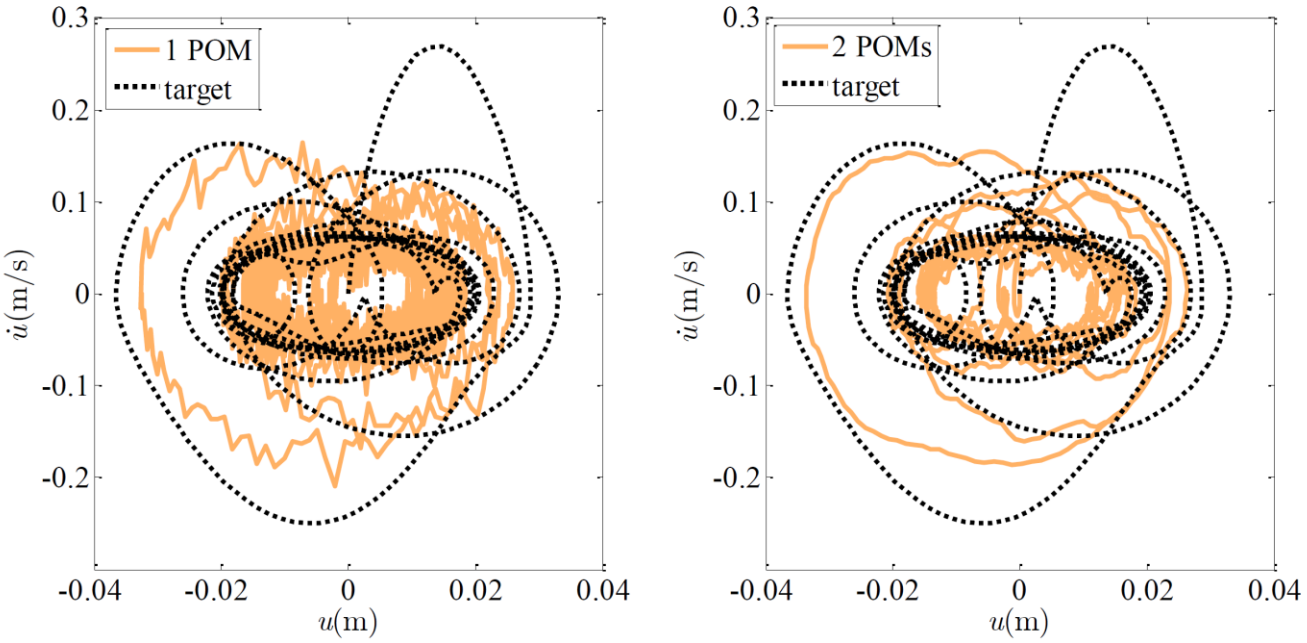

Figure 13. Damage $d = 0.5$ located at the inter-story between fourth and fifth floors: phase-space plots relevant to the fifth floor, and comparison among the target solution (black dotted line) and estimated ones (orange lines) for (left) $l = 1$ and (right) $l = 2$.

Table 1. Algorithm for the cuncurrent dual estimation of the ROM, and subspace update.

- At time t_0:
  1. Initialization of state and its covariance: $\widehat{\boldsymbol{\chi}}_0$, $\boldsymbol{\mathcal{P}}_0$
  2. Initialization of subspace and its covariance: $\widehat{\boldsymbol{\Xi}}_{l,0}$, $\boldsymbol{\Pi}_0$

- At time t_k, for $k = 1, \dots, N$:
  - Prediction stage:
    1. Prediction of state and its covariance:

$$\boldsymbol{\chi}_k^- = \boldsymbol{\psi}_k(\widehat{\boldsymbol{\chi}}_{k-1})$$
$$\boldsymbol{\mathcal{P}}_k^- = \boldsymbol{\mathcal{F}}_k \boldsymbol{\mathcal{P}}_{k-1} \boldsymbol{\mathcal{F}}_k^T + \boldsymbol{V}^{\chi}$$

       where $\boldsymbol{\mathcal{F}}_k = \frac{\partial \boldsymbol{\psi}_k(\chi)}{\partial \chi}\Big|_{\chi=\widehat{\chi}_{k-1}}$

    2. Prediction of subspace and its covariance:

$$\boldsymbol{\Xi}_{l,k}^- = \widehat{\boldsymbol{\Xi}}_{l,k-1}$$
$$\boldsymbol{\Pi}_k^- = \boldsymbol{\Pi}_{k-1} + \boldsymbol{V}^{\varphi}$$

  - Update stage:
    1. Computation of Kalman gains:

$$\boldsymbol{G}_{\chi,k} = \boldsymbol{\mathcal{P}}_k^- \boldsymbol{\mathcal{L}}_k^{\mathrm{T}} \boldsymbol{H}^{\mathrm{T}} \left(\boldsymbol{H} \boldsymbol{\mathcal{L}}_k \boldsymbol{\mathcal{P}}_k^- \boldsymbol{\mathcal{L}}_k^{\mathrm{T}} \boldsymbol{H}^{\mathrm{T}} + \boldsymbol{V}^{y} \right)^{-1}$$
$$\boldsymbol{G}_{\varphi,k} = \boldsymbol{\Pi}_k^- \boldsymbol{\mathcal{H}}^{\mathrm{T}} (\boldsymbol{\mathcal{H}} \boldsymbol{\Pi}_k^- \boldsymbol{\mathcal{H}}^{\mathrm{T}} + \boldsymbol{V}^{y})^{-1}$$

    2. Update of state and its covariance:

$$\widehat{\boldsymbol{\chi}}_k = \boldsymbol{\chi}_k^- + \boldsymbol{G}_{\chi,k} (\boldsymbol{y}_k - \boldsymbol{H} \boldsymbol{\mathcal{L}}_k \boldsymbol{\chi}_k^-)$$
$$\boldsymbol{\mathcal{P}}_k = \boldsymbol{\mathcal{P}}_k^- - \boldsymbol{G}_{\chi,k} \boldsymbol{H} \boldsymbol{\mathcal{L}}_k \boldsymbol{\mathcal{P}}_k^-$$

    3. Update of subspace and its covariance:

$$\widehat{\boldsymbol{\Xi}}_{l,k} = \boldsymbol{\Xi}_{l,k}^- + \boldsymbol{G}_{\varphi,k} \left(\boldsymbol{y}_k - \boldsymbol{\mathcal{H}} \boldsymbol{\Xi}_{l,k}^- \right)$$
$$\boldsymbol{\Pi}_k = \boldsymbol{\Pi}_k^- - \boldsymbol{G}_{\varphi,k} \boldsymbol{\mathcal{H}} \boldsymbol{\Pi}_k^-$$

Table 2. Computational complexity of each stage of the proposed algorithm (for stage indices, see Table 1).

	stage	Computational Complexity (Flops)
prediction	1	$O\left(\left(l+N_p\right)^3\right)$
	2	$O(m^2)$
update	1	$O\left(n^3+n\left(l+N_p\right)^2+n\left(3l+N_p\right)^2+n^2\left(3l+N_p\right)+n\left(3n+N_p\right)\left(3l+N_p\right)+lmn^2+(lm)^2\,n\right)$
	2	$O\left(n\left(3l+N_p\right)\left(3m+N_p\right)+\left(3l+N_p\right)^3\right)$
	3	$O(lmn^2+(l\,m)^2\,n)$

Table 3. Effect of the order l of the ROM on its accuracy, as measured via index p for both the undamaged and damaged states, and on the analysis speed-up, as provided by computational complexity and CPU time.

order	accuracy		speed-up	
l	$p_{\text{undamaged}}$	p_{damaged}	computational complexity	CPU time
1	99.983 %	99.894 %	22.6	6.5
2	99.999 %	99.999 %	8.6	4.4